

Article

**Discovery and Lead-optimization of 4,5-Dihydropyrazoles as Mono-Kinase Selective, Orally Bioavailable and Efficacious Inhibitors of Receptor Interacting Protein 1 (RIP1) Kinase**

Philip A. Harris, Nicolas Faucher, Nicolas George, Patrick M Eidam, Bryan W. King, Gemma White, Niall A Anderson, Deepak Bandyopadhyay, Allison M. Beal, Veronique BENETON, Scott B. Berger, Nino Campobasso, Sebastien Campos, Carol A. Capriotti, Julie A Cox, Alain DAUGAN, Frederic DONCHE, Marie-Helene Fouchet, Joshua N. Finger, brad geddes, Peter J. Gough, Pascal Grondin, Bonnie Hoffman, Sandra J Hoffman, Susan Hutchinson, Jae U Jeong, Emilie JIGOREL, Pauline Lamoureux, Lara K Leister, John D Lich, Mukesh K. Mahajan, Jamel Meslamani, Julie E. Mosley, Rakesh Nagilla, Pamela Nassau, Sze-Ling Ng, Michael T. Ouellette, Kishore Pasikanti, Florent POTVAIN, Michael A. Reilly, Elizabeth J. Rivera, stephane SAUTET, Michelle C Schaeffer, Clark A. Sehon, Helen H. Sun, James H. Thorpe, Rachel D Totoritis, Paris Ward, Natalie Wellaway, David D Wisnoski, James M. Woolven, John Bertin, and Robert W Marquis

*J. Med. Chem.*, **Just Accepted Manuscript** • DOI: 10.1021/acs.jmedchem.9b00318 • Publication Date (Web): 23 Apr 2019

Downloaded from <http://pubs.acs.org> on April 23, 2019

**Just Accepted**

"Just Accepted" manuscripts have been peer-reviewed and accepted for publication. They are posted online prior to technical editing, formatting for publication and author proofing. The American Chemical Society provides "Just Accepted" as a service to the research community to expedite the dissemination of scientific material as soon as possible after acceptance. "Just Accepted" manuscripts appear in full in PDF format accompanied by an HTML abstract. "Just Accepted" manuscripts have been fully peer reviewed, but should not be considered the official version of record. They are citable by the Digital Object Identifier (DOI®). "Just Accepted" is an optional service offered to authors. Therefore, the "Just Accepted" Web site may not include all articles that will be published in the journal. After a manuscript is technically edited and formatted, it will be removed from the "Just Accepted" Web site and published as an ASAP article. Note that technical editing may introduce minor changes to the manuscript text and/or graphics which could affect content, and all legal disclaimers and ethical guidelines that apply to the journal pertain. ACS cannot be held responsible for errors or consequences arising from the use of information contained in these "Just Accepted" manuscripts.



**ACS Publications**

is published by the American Chemical Society, 1155 Sixteenth Street N.W., Washington, DC 20036

Published by American Chemical Society. Copyright © American Chemical Society. However, no copyright claim is made to original U.S. Government works, or works produced by employees of any Commonwealth realm Crown government in the course of their duties.

1  
2  
3  
4  
5  
6  
7  
8  
9  
10  
11  
12  
13  
14  
15  
16  
17  
18  
19  
20  
21  
22  
23  
24  
25  
26  
27  
28  
29  
30  
31  
32  
33  
34  
35  
36  
37  
38  
39  
40  
41  
42  
43  
44  
45  
46  
47  
48  
49  
50  
51  
52  
53  
54  
55  
56  
57  
58  
59  
60

	Rivera, Elizabeth; GlaxoSmithKline USA SAUTET, stephane; Oncodesign Biotechnology, Schaeffer, Michelle; GlaxoSmithKline USA Sehon, Clark; GlaxoSmithKline USA Sun, Helen; GlaxoSmithKline USA Thorpe, James; GlaxoSmithKline Research and Development Totoritis, Rachel; GlaxoSmithKline USA Ward, Paris; GlaxoSmithKline USA Wellaway, Natalie; GlaxoSmithKline Research and Development Wisnoski, David; GlaxoSmithKline USA Woolven, James; GlaxoSmithKline Research and Development Bertin, John; GlaxoSmithKline USA Marquis, Robert; GlaxoSmithKline USA

SCHOLARONE™  
Manuscripts

# Discovery and Lead-optimization of 4,5-Dihydropyrazoles as Mono-Kinase Selective, Orally Bioavailable and Efficacious Inhibitors of Receptor Interacting Protein 1 (RIP1) Kinase

*Philip A. Harris,<sup>\*,†</sup> Nicolas Faucher,<sup>§</sup> Nicolas George,<sup>§</sup> Patrick M. Eidam,<sup>†</sup> Bryan W. King,<sup>‡</sup> Gemma V. White,<sup>#</sup> Niall A. Anderson,<sup>#</sup> Deepak Bandyopadhyay,<sup>‡</sup> Allison M. Beal,<sup>†</sup> Veronique Beneton,<sup>§</sup> Scott B. Berger,<sup>†</sup> Nino Campobasso,<sup>‡</sup> Sebastien Campos,<sup>#</sup> Carol A. Capriotti,<sup>†</sup> Julie A. Cox,<sup>‡</sup> Alain Daugan,<sup>§</sup> Frederic Donche,<sup>§</sup> Marie-Hélène Fouchet,<sup>§</sup> Joshua N. Finger,<sup>†</sup> Brad Geddes,<sup>†</sup> Peter J. Gough,<sup>†</sup> Pascal Grondin,<sup>§</sup> Bonnie L. Hoffman,<sup>†</sup> Sandra J. Hoffman,<sup>†</sup> Susan E. Hutchinson,<sup>#</sup> Jae U. Jeong,<sup>†</sup> Emilie Jigorel,<sup>§</sup> Pauline Lamoureux,<sup>§</sup> Lara K. Leister,<sup>†</sup> John D. Lich,<sup>†</sup> Mukesh K. Mahajan,<sup>†</sup> Jamel Meslamani,<sup>‡</sup> Julie E Mosley,<sup>#</sup> Rakesh Nagilla,<sup>†</sup> Pamela M Nassau,<sup>#</sup> Sze-Ling Ng,<sup>†</sup> Michael T. Ouellette,<sup>‡</sup> Kishore K. Pasikanti,<sup>†</sup> Florent Potvain,<sup>§</sup> Michael A. Reilly,<sup>†</sup> Elizabeth J. Rivera,<sup>†</sup> Stéphane Sautet,<sup>§</sup> Michelle C. Schaeffer,<sup>†</sup> Clark A. Sehon,<sup>†</sup> Helen Sun,<sup>†</sup> James H. Thorpe,<sup>#</sup> Rachel D. Totoritis,<sup>‡</sup> Paris Ward,<sup>‡</sup> Natalie Wellaway,<sup>#</sup> David D. Wisnoski,<sup>‡</sup> James M. Woolven,<sup>#</sup> John Bertin<sup>†</sup> and Robert W. Marquis<sup>†</sup>*

<sup>†</sup>Pattern Recognition Receptor DPU and <sup>‡</sup>Platform Technology & Science, GlaxoSmithKline, Collegeville Road, Collegeville, Pennsylvania 19426, United States. <sup>#</sup>Flexible Discovery unit,

GlaxoSmithKline, Gunnels Wood Road, Stevenage, Hertfordshire SG1 2NY, UK. §Flexible  
Discovery unit, GlaxoSmithKline, 25-27 avenue du Québec, 91951, Les Ulis cedex, France.

## ABSTRACT

RIP1 kinase regulates necroptosis and inflammation and may play an important role in contributing to a variety of human pathologies, including inflammatory and neurological diseases. Currently RIP1 kinase inhibitors have advanced into early clinical trials for evaluation in inflammatory diseases such as psoriasis, rheumatoid arthritis and ulcerative colitis, and neuro-logical diseases such as amyotrophic lateral sclerosis (ALS) and Alzheimer's disease. In this paper we report on the design of potent and highly selective dihydropyrazole (DHP) RIP1 kinase inhibitors starting from a high-throughput screen and the lead-optimization of this series from a lead with minimal rat oral exposure to the identification of dihydropyrazole **77** with good pharmacokinetic profiles in multiple species. Additionally, we identified a potent murine RIP1 kinase inhibitor **76** as a valuable in vivo tool molecule suitable for evaluating the role of RIP1 kinase in chronic models of disease. DHP **76** showed efficacy in mouse models of both multiple sclerosis and human retinitis pigmentosa.

## INTRODUCTION

Over the past decade, Receptor Interacting Protein 1 (RIP1) kinase activity has emerged as the master regulator of a newly identified form of cell death termed necroptosis.<sup>1</sup> Necroptosis, like apoptosis, is a programmed and highly orchestrated form of cell death which is important for organismal development and homeostasis.<sup>2,3</sup> However, unlike apoptosis which is largely

1  
2  
3 quiescent, necroptosis results in a highly pro-inflammatory response which is thought to underpin  
4  
5 multiple human pathologies.<sup>4</sup> Although RIP1 kinase driven necroptosis was originally identified  
6  
7 downstream of TNFR1 activation, work over the last few years has shown that RIP1 kinase activity  
8  
9 can also be activated in response to various other cellular signals including activation of other  
10  
11 death receptors (TRAIL, FAS), toll-like receptors (TLR3, TLR4) and some forms of cellular  
12  
13 stress.<sup>5-7</sup> Furthermore, although RIP1 kinase activity was originally shown to be critical for driving  
14  
15 necroptosis, additional work has now shown that RIP1 kinase enzymatic activity can also be a  
16  
17 direct regulator of pathogenic forms of apoptosis and pro-inflammatory cytokine production.<sup>8,9</sup>  
18  
19 Based on the multiple signaling path-ways that can drive RIP1 kinase activity and the potential for  
20  
21 multiple inflammatory outputs, inhibitors of this RIP1 kinase pathway have the potential for a  
22  
23 broad therapeutic footprint to treat multiple inflammatory diseases.  
24  
25  
26

27  
28 Degtarev et al. identified several series of RIP1 kinase inhibitors using a phenotypic cell screen  
29  
30 that measured their ability to block necrotic death induced by treatment with a combination of TNF  
31  
32 and the caspase inhibitor zVAD.fmk.<sup>10,11</sup> The most studied inhibitor, indole-hydantoin **1** (known  
33  
34 as Nec-1s or 7-Cl-O-Nec-1, see Figure 1), was subsequently co-crystallized in the RIP1 kinase  
35  
36 domain showing it to occupy an allosteric lipophilic pocket at the back of the ATP binding site.<sup>12</sup>  
37  
38 This allosteric type III binding mode resulted in an excellent kinase selectivity profile.<sup>13</sup> Our screen  
39  
40 of a GSK library of kinase inhibitors collected from prior kinase programs identified a number of  
41  
42 potent RIP1 kinase inhibitors belonging to the type II class, which are known to target a conserved  
43  
44 “DFG-out” inactive conformation of the kinase, as exemplified by **2**.<sup>14</sup> This conserved DFG  
45  
46 sequence is located immediately before the kinase activation loop and in RIP1 this sequence is the  
47  
48 more rarely observed DLG. In parallel, a separate DNA-encoded library screen led to the  
49  
50 identification of a novel and highly kinase selective benzoxazepinone RIP1 kinase inhibitor  
51  
52  
53  
54  
55  
56  
57  
58  
59  
60

template, exemplified by **3**.<sup>15</sup> The co-crystal structure of **3** in the RIP1 kinase domain showed it occupied the same allosteric binding pocket as the indole-hydantoin **1**. A favorable developability profile and complete kinase specificity for RIP1 led us to select this series for lead-optimization. This effort resulted in selection of development candidate **4**, known as GSK2982772, which is currently under evaluation in phase 2a clinical trials in psoriasis, rheumatoid arthritis and ulcerative colitis patients.<sup>16</sup> Recently, Yoshikawa et al. have disclosed a benzoxazepinone analog **5** with a higher brain penetration and efficacy in a mouse experimental autoimmune encephalomyelitis (EAE) model of multiple sclerosis.<sup>17</sup>

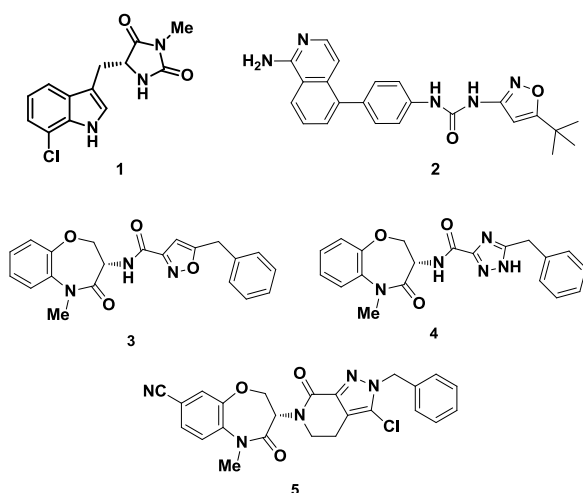


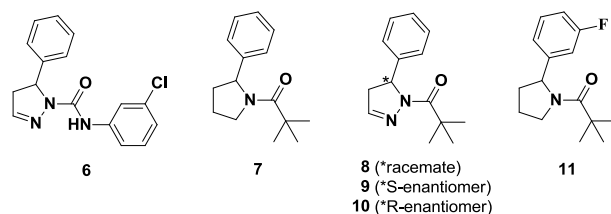
**Figure 1.** Structure of RIP1 kinase inhibitors

## RESULTS AND DISCUSSION

RIP1 kinase type III inhibitors, exemplified by both indole-hydantoin **1** and benzoxazepinone **3**, offer clear advantages as starting points for drug discovery in terms of their RIP1 kinase specificity, combined with more favorable physicochemical profiles, such as solubility, lipophilicity and protein binding, compared to type II inhibitors such as **2**. To identify additional novel chemotypes targeting this allosteric pocket type in RIP1 kinase we initiated a high-throughput screen (HTS) of

the GSK compound collection. From this HTS, two hits, a dihydropyrazole urea **6** and a pyrrolidine pivalate **7**, were of particular interest, as they possessed sub-micromolar activity in both a RIP1 kinase fluorescence polarization (FP) binding assay and a cellular assay of necrotic human U937 cell death (Table 1). Inhibitors **6** and **7** share a common acyl benzylamine pharmacophore and a hybrid dihydropyrazole (DHP) pivalate **8** was prepared in an effort to bridge these two series. This hybrid DHP **8** showed a significant increase in both RIP1 kinase FP activity (12-fold) and U937 cellular efficacy (40-fold). As the potency of **8** was approaching the lower limit of sensitivity in the RIP1 kinase FP binding assay, the biochemical activity was profiled in an ADP-Glo tight binding assay revealing its potency to be in the low nanomolar range. A clear stereochemical dependence was observed as the (*S*) enantiomer **9** was active, compared to the inactive (*R*) enantiomer **10**. Consistent with the type III binding mode, DHP **9** showed no additional activity when profiled against 339 other human kinases in a P33 radiolabeled assay screen at Reaction Biology Corporation at 10  $\mu$ M (see Supporting Information).

**Table 1. RIP1 kinase HTS Screening Hits and Hybrid**



Cpd	RIP1 FP <sup>a,b</sup>	ADP-Glo <sup>a</sup>	U937 cell <sup>a</sup>	LE <sup>c</sup>
	IC <sub>50</sub> (nM)	IC <sub>50</sub> (nM)	IC <sub>50</sub> (nM)	
6	126	-	398	0.46
7	316	-	316	0.53

8	25	4.8	8	0.69
9	16	1.6	4	0.73
10	>10,000	>10,000	>10,000	—
11	200	-	79	

<sup>a</sup>Assay protocols are described in Supporting Information; IC<sub>50</sub> values are the average of at least two determinations. <sup>b</sup>Lower limit of sensitivity is ca. 10 nM. <sup>c</sup>Ligand efficiency (LE) based on RIP1 FP (**6,7**) and ADP-Glo potency (**8,9**) and is derived from  $LE = 1.4(pIC_{50})/N$ , where N is the number of non-hydrogen atoms.

In general, the DHP inhibitors such as the pivalate **8** were about 10-fold more potent than their pyrrolidine analogs, such as pivalate **7**. The DHP ring of **8** has less conformational flexibility than the saturated pyrrolidine of **7** and the additional nitrogen atom acts to restrict the torsional angle around the carbonyl group, thus holding the inhibitor in conformations that are likely more favorable for binding to RIP1. Although we did not progress the pyrrolidine series, we were able to successfully crystallize the meta-fluorophenyl pyrrolidine pivalate **11** in the RIP1 kinase domain confirming this pharmacophore occupies the same allosteric pocket in the back of the ATP pocket as indole-hydantoin **1** (Figure 2a). The inhibitor makes no interaction with the kinase hinge but the pivaloyl carbonyl of **11** makes a H-bond to the backbone of Asp156 (Figure 2b).



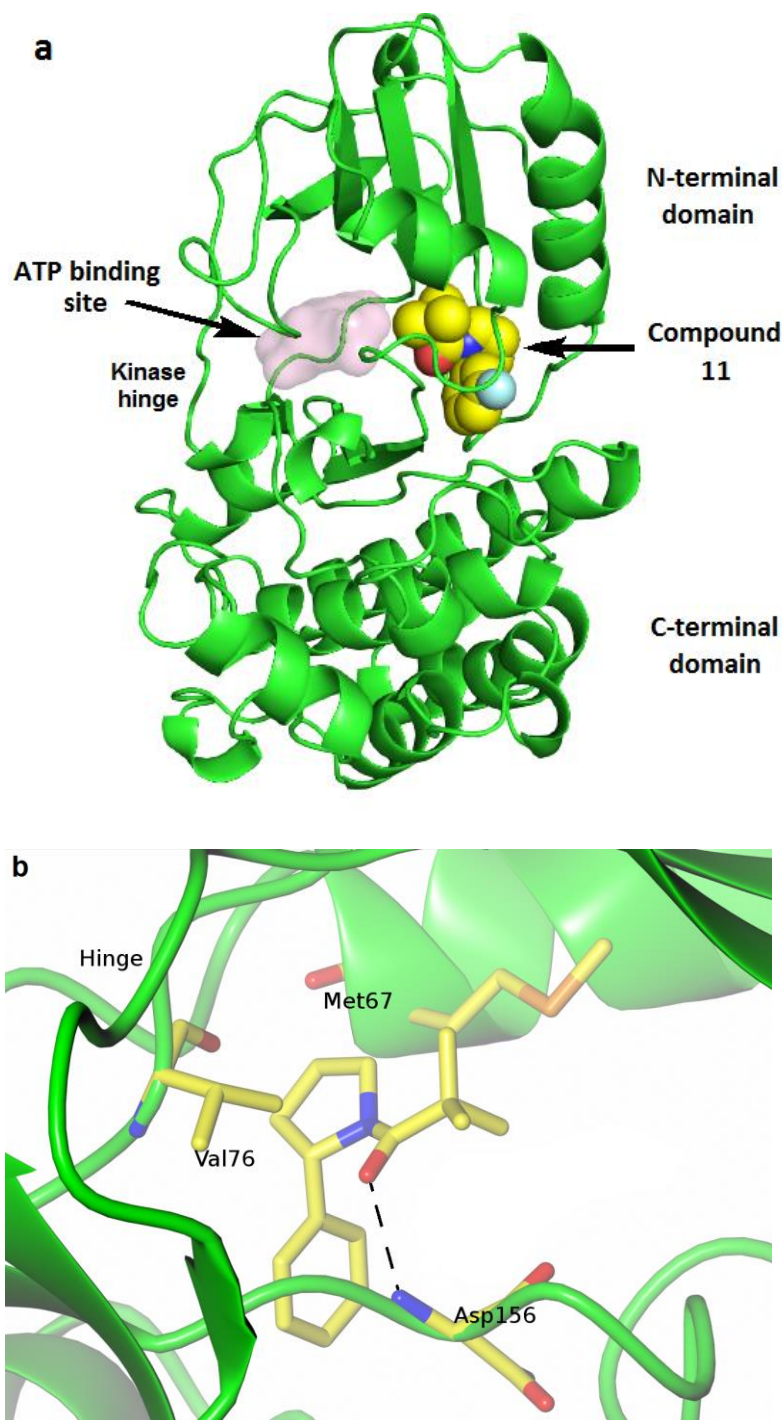


**Figure 2.** a) Co-crystal structure of RIP1 (1-294, C34A, C127A, C233A, and C240A) and pyrrolidine pivalate **11**. The inhibitor **11**, represented as spheres with color coding: carbon (yellow), nitrogen (blue), oxygen (red), fluorine (green), occupies an allosteric region distinct from the ATP binding pocket, which is shaded in pink. b) Close-up view of **11** bound in the allosteric

pocket; the amide carbonyl of **11** makes a direct hydrogen-bond interaction with the backbone amide NH of Asp156. Coordinates and structure factors for this cocrystal structure have been deposited in the Protein Data Bank with the accession numbers 6OCQ.

The excellent potency and kinase selectivity of the RIP1 kinase inhibitor **9**, combined with its inactive enantiomer as a negative control, made it an excellent in vitro tool for evaluating the in vitro biology of RIP1 kinase.<sup>18</sup> The main goal of the initial lead optimization was to improve the pharmacokinetic profile of this series as **9** possessed minimal oral exposure in rats. Additionally, despite being a highly efficient ligand ( $LE = 0.73$ ), inhibitor **9** exhibited a high  $\log P$  of 5.9 resulting in a suboptimal lipophilic ligand efficiency ( $pIC_{50} - \log P$ ) of 2.9 and thus reducing lipophilicity was also desirable.

We previously reported that type III RIP1 kinase inhibitors such as **3** and **4** demonstrate a species selectivity for inhibition of primate RIP1 kinase compared to non-primate RIP1 kinase.<sup>15</sup> Consistent with this observation, inhibitors from this DHP series, as exemplified by **9** in Table 2, exhibited approximately equivalent RIP1 kinase FP potency against human and monkey RIP1 kinase, but were significantly less potent against rodent, minipig, rabbit and dog RIP1 kinase. This species selectivity was not observed with any of the type II “DFG-out” RIP1 kinase inhibitors we previously profiled (for example **2**) but appears to be reserved for this type III binding mode. As detailed in our prior report, selectively mutating key amino acids in the mouse RIP1 kinase activation loop, where non-primate differed from primate, increases the potency of benzoxazepinone **3** in mouse cells to that approaching human.<sup>15</sup> This suggests the murine RIP1 kinase activation loop lacks the flexibility to adopt the preferred conformation required for optimal binding of type III inhibitors.

**Table 2. RIP1 kinase Species Selectivity of Compound 9**

Species	RIP1 FP	Fold
	IC <sub>50</sub> (nM) <sup>a</sup>	
Human	40 <sup>b</sup>	1
Monkey	32 <sup>b</sup>	0.8
Mouse	631	16
Rabbit	1585	40
Minipig	2512	63
Rat	5012	125
Dog	5012	125

<sup>a</sup>Data reported for side-by-side experiments (n=4, except mouse n=2). <sup>b</sup>Values at the lower limit of sensitivity (ca. 10 nM).

Route of clearance studies in rat for DHP **9** demonstrated a high systemic clearance, greater than liver blood flow, but no excretion via renal or biliary routes. The oral exposure in rat at 2 mg/kg was below the limit of detection. The observed clearance was attributed to metabolism, with hydroxylation at the 3-position of the DHP ring detected in rat blood, bile and urine, along with other hydroxylated regioisomers of unconfirmed identity. This was consistent with high in vitro metabolism observed in rat liver microsomes as evidenced by short half-lives (Table 3). In vitro metabolite identification in rat, dog, monkey and human liver microsomes confirmed that the parent was extensively metabolized, as detailed in Figure 3. The major metabolite (M246d) in rat and dog resulted from hydroxylation on the DHP ring. The 3-hydroxylated metabolite (M246a) was formed only in low levels. In human liver microsomes the major metabolite was hydroxylation at the *tert*-butyl group (M246c). No human unique metabolites were observed for DHP **9**. A small amount of metabolite (M246b) from oxidation at the phenyl ring occurred and no pyrazole

metabolite (**14**) was detected in any species. Bis-hydroxylation metabolites (M262a,b,c) were also observed in all species, most predominantly in monkey, along with a trihydroxylation/reduction metabolite (M276).

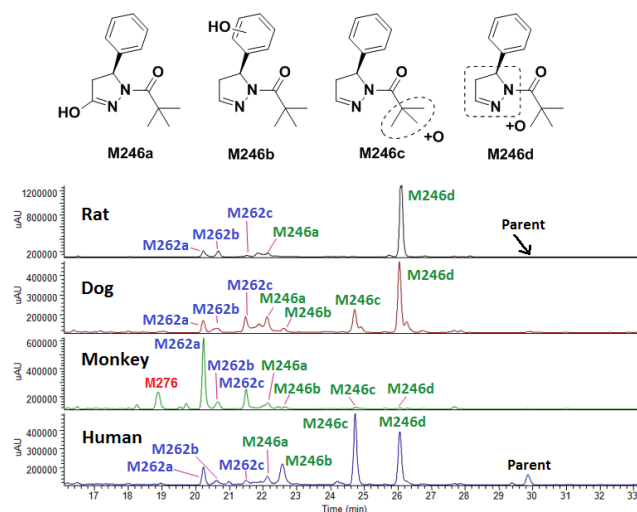
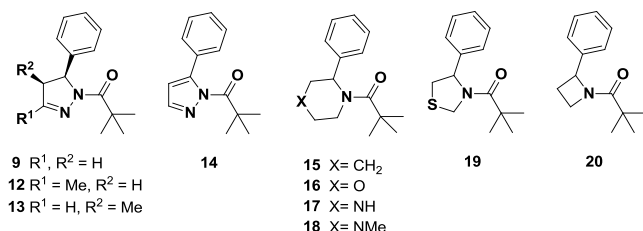


**Figure 3.** Metabolite identification of DHP **9** in rat, dog, monkey, human liver microsomes. Hydroxylated metabolites are labeled in green, bis-hydroxylation metabolites in blue and a trihydroxylation/reduction metabolite in red. Structural assignments for metabolites were made tentatively based upon mass spectral fragmentation pattern.

Our initial SAR investigations around modifying or replacing the DHP heterocycles met with limited success, as shown in Table 3. Addition of methyl groups to the ring (**12**, **13**) or aromatization of the ring (**14**) led to reduction in potency and no improvement in intrinsic clearances. Replacement of the DHP ring with 6-membered ring analogs (**15-18**) or a thiazoline (**19**) were significantly less active in our assays; however, the smaller azetidine replacement (**20**) retained moderate activity. Zhang et al. have recently disclosed an analogous series of RIP1 kinase inhibitors with a variety of heterocyclic modifications of the core ring.<sup>19</sup> The restricted SAR with regards to alterations to the heterocycle support the observations in the co-crystal structure of **11**

locating the inhibitor in a narrow lipophilic pocket. Changes in this central ring that result in alterations in the conformation of the aryl and amide groups were less optimal for inhibitor binding.

**Table 3. Replacements or Modifications of the DHP Heterocycle**



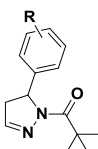
Cpd	RIP1 FP <sup>a</sup> IC <sub>50</sub> (nM)	cell U937 <sup>a</sup> IC <sub>50</sub> (nM)	CHI Log <i>D</i> <sup>b</sup>	Microsome/hepatocyte t <sub>1/2</sub> (min.) <sup>c</sup>	
				rat	human
9	16	4	5.8	3.5	20
12	126	159	6.4	2.5	37
13	200	400	6.5	12	27
14	>10,000	>10,000	8.3		
15	>10,000	>10,000	6.7		
16	>10,000	>1,000	4.7		
17	>10,000	>10,000	2.5		
18	>10,000	>10,000	4.9		
19	3,980	>1,000	5.6	3.2	18
20	79	126	5.0	30	>165

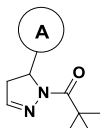
<sup>a</sup>Assay protocols are described in Supporting Information; IC<sub>50</sub> values are the average of at least two determinations. <sup>b</sup>CHI (chromatographic hydrophobicity index) log *D* at pH 7.4 was calculated from the retention time (*t<sub>R</sub>*) observed in a fast gradient reverse-phase HPLC. <sup>c</sup>Microsome half-lives reported for **9**, **13** and **19**, hepatocyte half-lives for **12** and **20**.

We next examined changes around the aryl ring. Small lipophilic groups such as methyl and fluoro (e.g. **21-25**) retained potency comparable to **8**, albeit with no improvements in intrinsic

clearance (Table 4). Bulkier substitutions, such as *tert*-butyl (e.g. **27**) or more polar groups (e.g. **28**) were less tolerated. Replacement of the phenyl ring with more polar heterocycles such as pyridines (**29-31**), pyrazole (**32**), imidazole (**33**) and oxazole (**34**) were detrimental to potency. Despite their drop in potency it was encouraging that the pyridine (**29, 30**) and oxazole analog **34** did show significantly improved stability in microsomes. Nonpolar cyclohexyl (**35**) or cyclopentyl (**36**) replacements had moderate potency; whereas more polar aliphatic heterocycles such as tetrahydropyran (**37**) and N-methylpiperidine (**38**) were inactive in our assays.

**Table 4. Substitution or Replacements of the Phenyl Ring**





<b>8</b> H	<b>25</b> 4-Cl	<b>29</b> 2-pyridyl	<b>34</b> 4-oxazolyl
<b>21</b> 3-F	<b>26</b> 3-Cl	<b>30</b> 3-pyridyl	<b>35</b> cyclohexyl
<b>22</b> 3-F, 4-Me	<b>27</b> 4- <i>t</i> -Bu	<b>31</b> 4-pyridyl	<b>36</b> cyclopentyl
<b>23</b> 3,5-di-F	<b>28</b> 4-SO <sub>2</sub> Me	<b>32</b> pyrazol-3-yl	<b>37</b> 4-tetrahydropyran
<b>24</b> 4-Me		<b>33</b> imidazol-4-yl	<b>38</b> 4-N-methylpiperidine

Cpd	FP/ADP-Glo <sup>a,b</sup> IC <sub>50</sub> (nM)	cell U937 <sup>a</sup> IC <sub>50</sub> (nM)	CHI Log <i>D</i> <sup>c</sup>	microsome t <sub>1/2</sub> (min.)	
				rat	human
8	4.8	8	5.8		
21	0.5	4	5.9		
22	2	2.5	6.6	2.6	16
23	1.3	6.4	6.3		
24	6.3	4	6.4	2.3	22
25	6.3	13	6.6	8.7	26
26	9	63	6.6	3.0	8.3
27	3,980	>1,000	8.0		

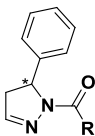
28	2,000	>1,000	4.1		
29	316	398	3.5	79	>90
30	159	126	3.2	>90	>90
31	5,012	>1,000	3.2		
32	3,980	>1,000	2.7		
33	3,980	5,012	1.7		
34	794	1000	3.0	>90	>90
35	126	794	7.3	<1.4	5.8
36	200	794	6.7	2.6	5.9
37	>10,000	>1,000	4.1		
38	>10,000	>1,000	1.4		

<sup>a</sup>Assay protocols are described in Supporting Information; IC<sub>50</sub> values are the average of at least two determinations. <sup>b</sup>RIP1 FP binding assay was used to assess the potency of inhibitors with an IC<sub>50</sub> ca. > 10 nM; whereas for more potent inhibitors where the limit of sensitivity FP assay was reached, the ADP-Glo tight binding analyses were employed to more accurately determine potency. <sup>c</sup>CHI (chromatographic hydrophobicity index) log D at pH 7.4 was calculated from the retention time (t<sub>R</sub>) observed in a fast gradient reverse-phase HPLC.

The inhibitor **11** bound in the RIP1 kinase allosteric binding pocket showed the pivalate group orientated towards the opening of the pocket suggesting this area would have more space for optimization. Our initial SAR exploration around this region is summarized in Table 5. Reducing the size of the *tert*-butyl group or adding heteroatoms reduced potency as exemplified by DHPs **39-41**. Cyclizing the aliphatic group led to potent analogs (**42-44**) but did not improve the microsomal stability. The heterocycles tetrahydropyran and tetrahydrofuran (**45**, **46**) were less active; however, **45** showed encouragingly improved intrinsic stability. Replacing the *tert*-butyl moiety with aryl groups represented by DHPs **47-50** was less favorable regarding potency. The N-methylpiperidine **51** lost activity in our assays, indicating that a protonatable amine in this region, as with analog **41**, is not favorable with the lipophilic environment. However, reduction of the

nitrogen basicity, as seen with the N-phenylpiperidine **52** and N-acetylpiperidine **53** analogs, led to recovery of the potency. The N-acetylpiperidine active *S*-enantiomer **54** was prepared and proved to be both potent and stable in rat and human liver microsomes.

**Table 5. Substitution or Replacements of the *tert*-Butyl**



<b>8</b> t-butyl	<b>44</b> cyclobutyl	<b>50</b> 2-pyridyl
<b>39</b> i-propyl	<b>45</b> 4-tetrahydropyran	<b>51</b> 4-N-methylpiperidine
<b>40</b> t-butyl-2-ol	<b>46</b> 3-tetrahydrofuran	<b>52</b> 4-N-phenylpiperidine
<b>41</b> t-butyl-2-amine	<b>47</b> phenyl	<b>53</b> 4-N-acetylpiperidine (*racemate)
<b>42</b> cyclopentyl	<b>48</b> 4-pyridyl	<b>54</b> 4-N-acetylpiperidine (*S-enantiomer)
<b>43</b> cyclohexyl	<b>49</b> 3-pyridyl	

Cpd	FP/ADP-Glo <sup>a,b</sup> IC <sub>50</sub> (nM)	cell U937 <sup>a</sup> IC <sub>50</sub> (nM)	CHI Log <i>D</i> <sup>c</sup>	microsome t <sub>1/2</sub> (min.)	
				rat	human
8	4.8	8	5.8		
39	80	159	4.4	80	>90
40	631	501	3.4	55	>90
41	>10,000	>10,000	1.4		
42	16	63	5.4	12	68
43	1.6	13	5.9	5	37
44	126	200	4.7	35	83
45	316	794	3.1	>90	>90
46	1,000	>1,000	3.0		
47	398	794	4.6		
48	2,000	2,000	2.7		
49	2,512	2,000	2.7		
50	>10,000	>10,000	2.4		



51	>10,000	7,940	1.1		
52	13	79	6.3	15	>90
53	126	501	2.5		
54	35	126	2.5	>165	>165

<sup>a</sup>Assay protocols are described in Supporting Information; IC<sub>50</sub> values are the average of at least two determinations. <sup>b</sup>RIP1 kinase FP binding assay was used to assess the potency of inhibitors with an IC<sub>50</sub> ca. > 10 nM; whereas for more potent inhibitors where the limit of sensitivity FP assay was reached, the ADP-Glo tight binding analyses were employed to more accurately determine potency. <sup>c</sup>CHI (chromatographic hydrophobicity index) log D at pH 7.4 was calculated from the retention time (t<sub>R</sub>) observed in a fast gradient reverse-phase HPLC.

One clear trend that emerged is that decreased lipophilicity of the DHPs correlated to reduced microsomal intrinsic clearances, as demonstrated in Figure 4. Only DHPs **30**, **34**, **45** and **54**, each with a log D under 3.5, have greater than 90 min. half-lives in rat microsomes. The oral rat pharmacokinetic profile of these four DHPs is summarized in Table 6. Compared to DHP **9**, which had undetectable rat oral exposure, these all showed improved exposures, particularly DHP **54**, albeit still with a relatively short duration. From this initial round of SAR investigation, DHP **54** possessed a good combination of RIP1 potency, low intrinsic clearance and rat oral exposure to be evaluated in vivo. DHP **54** was also highly soluble as indicated by fasted state simulated intestinal fluid (FaSSIF) solubility of the crystalline form being 7.4 mg/mL after 4 h at 37 °C.

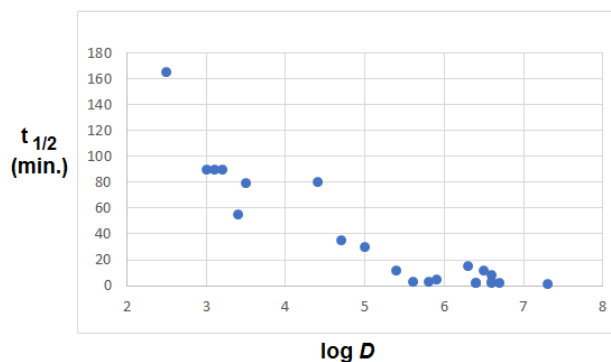


**Figure 4.** Comparison of chromatographic log *D* with rat liver microsome half-lives for DHPs in Tables 3-5.

**Table 6. Oral Pharmacokinetic Profiles of DHPS in Rat<sup>a</sup>**

Cpd	Cmax (ng/mL)	Tmax (min.)	AUC <sub>0-∞</sub> (μg·h/mL)
30	360	5	0.26
34	345	5	0.20
45	95	5	0.044
54	795	30	1.6

<sup>a</sup>Dosed at 2 mg/kg in 5% DMSO/6% Cavitron™ solution.

Despite the lower non-primate RIP1 activity characteristic of these type III inhibitors, we had sufficient murine cellular potency and exposure to examine this series in an acute in vivo mouse model evaluating protection from TNF induced lethal shock. DHP **54** exhibited moderate cellular activity against murine L929 (IC<sub>50</sub> 6.3 μM) in blockage of necrotic death induced by TNF plus the caspase inhibitor zVAD.fmk. In this in vivo model, injection of TNF plus zVAD.fmk leads to a systemic inflammatory response, characterized by hypotension, hepatitis, hypothermia and bowel necrosis.<sup>20</sup> Inhibitor **54** was dosed orally, at doses of 1.4, 14 and 140 mg/kg, 5 minutes prior to TNF/zVAD.fmk injection and showed 22, 43 and 96% protection from body temperature loss over 3 hours, respectively, compared to TNF/ zVAD.fmk alone (Figure 5). Assuming the efficacy is Cmax driven, the calculated IC<sub>50</sub> of 1.3 μM from this in vivo study correlated reasonably well with the observed in vitro murine cellular L929 IC<sub>50</sub> of 6.3 μM.

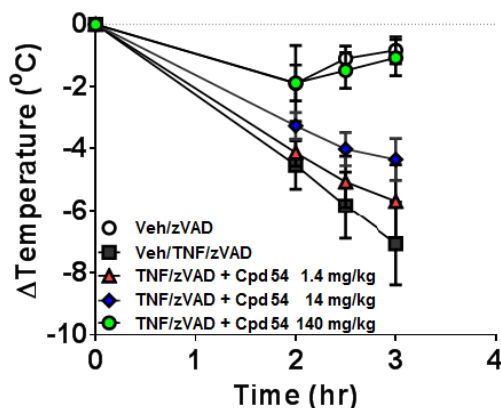
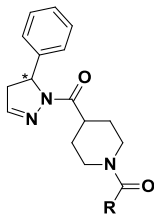


**Figure 5.** Evaluation of DHP **54** in the TNF/zVAD induced lethal shock mouse model at doses of 1.4, 14 and 140 mg/kg, measuring reduction in body temperature loss over time. Data are presented as the mean  $\pm$  SEM,  $*p < 0.05$ .

We next focused on modifying the N-acyl piperidine region of DHP **54** to further improve the profile as summarized in Table 7. Replacement of the methyl with trifluoromethyl (**55**) retained potency but diminished intrinsic stability; whereas larger or cycloalkyl groups reduced potency (**56**, **57**). Phenyl replacement (**58**) of the methyl was more potent but did not have microsomal stability. A series of heterocycles were also evaluated from which the most notable were the oxazoles (**61**, **62**) for their excellent cellular potency and the 4-pyrazole (**64**) and 1,2,3-triazole (**65**) for good intrinsic clearances. The rat IV pharmacokinetic profiles of the most promising DHPs are summarized in Table 8. These inhibitors show moderate volumes of distribution, moderate to high clearances and short half-lives in rat and therefore did not represent an improvement over DHP **54**. The good stability in rat microsomes for DHPs **54**, **62**, **64** and **65** did not translate into longer half-lives in rat. We therefore switched from evaluating intrinsic clearances in microsomes to hepatocytes, which, by the inclusion of phase 2 metabolic pathways, may provide an improved correlation.

Table 7. N-Acylpiperidine DHPs



- 55 trifluoromethyl

56 ethyl

57 cyclohexyl

58 phenyl
- 59 3-pyridyl

60 2-pyridyl

61 oxazol-4-yl

62 oxazol-5-yl (\*S-enantiomer)
- 63 pyrazol-3-yl

64 pyrazol-4-yl

65 1,2,3-triazole

66 4-thiazole (\*S-enantiomer)

Cpd	FP/ADP-Glo <sup>a,b</sup> IC <sub>50</sub> (nM)	cell U937 <sup>a</sup> IC <sub>50</sub> (nM)	CHI Log <i>D</i> <sup>b</sup>	Microsome t <sub>1/2</sub> (min.)	
				rat	human
54	35	126	2.5	>165	>165
55	16	160	4.9	29	>90
56	126	316	3.2	64	>165
57	794	2511	5.4		
58	10	79	4.4	5	103
59	159	316	2.6		
60	2.5	316	3.1		
61	6.3	7.9	2.9	32	>165
62	2.5	10	2.7	>180	>180
63	25	100	2.4	19	>165
64	79	251	2.1	>165	>165
65	32	159	2.0	>165	>165
66	20	16	3.0	39	>180

<sup>a</sup>Assay protocols are described in Supporting Information; IC<sub>50</sub> values are the average of at least two determinations. <sup>b</sup>RIP1 FP binding assay was used to assess the potency of inhibitors with an IC<sub>50</sub> ca. > 10 nM; whereas for more potent inhibitors where the limit of sensitivity FP assay was reached, the ADP-Glo tight binding analyses were employed to more accurately determine potency. <sup>b</sup>CHI (chromatographic hydrophobicity index) log *D* at pH 7.4 was calculated from the retention time (t<sub>R</sub>) observed in a fast gradient reverse-phase HPLC.

**Table 8. Rat IV Pharmacokinetic Profiles of DHPs<sup>a</sup>**

Cpd	Cl (mL/min/Kg)	V <sub>ss</sub> (L/Kg)	<i>t</i> <sub>1/2</sub> (min.)	AUC <sub>0-∞</sub> (μg·h/mL)
54	44	1.7	51	0.42
61	58	0.98	12	0.29
62	42	2.1	28	0.40
64	46	1.6	25	0.36
65	37	1.3	25	0.45

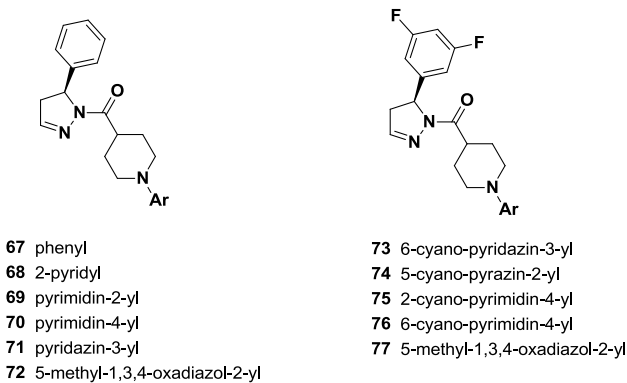
<sup>a</sup>Dosed at 1 mg/kg in 5% DMSO/20% Cavitron™ solution.

With no significant improvement over DHP **54** observed with N-acyl piperidine substitutions, we next explored replacement of the acyl group with an aryl or heterocyclic ring. The N-phenyl piperidine **67** showed an improvement in potency compared to **54** but this was accompanied by a significant increase in lipophilicity. Attachment of nitrogen heterocycles such as pyridine, pyrimidine and pyridazine (**68-71**) maintained the potency, reduced lipophilicity but lacked stability in rat hepatocytes. However, replacement with 5-methyl-1,3,4-oxazdiazole led to inhibitor **72** with good in vitro potency and improved stability in rat hepatocytes. The rat pharmacokinetic profile of **72** compared to **54** was significantly improved with a lower clearance and higher exposure, as shown in Table 10.

A consistent trend was that addition of 3,5-difluoro substitution to the aryl ring resulted in modest (~ 2-fold) improvement in potency in U937 cellular activity. Figure 6 shows this trend in a head-to-head comparison of unsubstituted phenyl-DHPs with their 3,5-difluorophenyl analogs. The fluorines are most likely providing additional Van der Waals contacts in the rear of the allosteric pocket where the aryl ring binds. A series of cyano substituted nitrogen heterocycles, as

represented by DHPs **73-76**, were also evaluated which showed excellent cellular potencies. Their rat intrinsic clearances were not as good as DHP **72**, which translated into higher rat in vivo clearances, as shown in Table 10 for DHPs **74** and **76**. Combining the more stable 5-methyl-1,3,4-oxazdiazole **72** with the 3,5-di-fluoro aryl substitution to improve cell potency led to DHP **77**. This DHP had good potency combined with full stability in both rat and human hepatocytes, which translated into a favorable rat pharmacokinetic profile with a low clearance, good exposure and good oral bioavailability.

**Table 9. N-Aryl-Piperidine Substitutions**



Cpd	FP/ADP-Glo <sup>a,b</sup> IC <sub>50</sub> (nM)	cell U937 <sup>a</sup> IC <sub>50</sub> (nM)	CHI Log <i>D</i> <sup>c</sup>	Hepatocyte t <sub>1/2</sub> (min.)	
				rat	human
54	35	126	2.5	>187	>187
67	16	25	6.3		
68	2.5	16	5.1	3.8	>187
69	1.6	10	4.7	8.2	>187
70	5	32	3.2	<24	198
71	20	50	3.4	<31	139

72	50	126	3.2	173	198
73	7.9	25	4.8	125	>480
74	2.0	7.9	5.2	107	198
75	2.5	2.0	5.1	55	126
76	1.0	4.0	5.0	69	198
77	20	63	3.6	198	198

<sup>a</sup>Assay protocols are described in Supporting Information; IC<sub>50</sub> values are the average of at least two determinations. <sup>b</sup>RIP1 FP binding assay was used to assess the potency of inhibitors with IC<sub>50</sub> > 10 nM; whereas for more potent inhibitors where the limit of sensitivity FP assay was reached, the ADP-Glo tight binding analyses were employed to more accurately determine potency. <sup>c</sup>CHI (chromatographic hydrophobicity index) log D at pH 7.4 was calculated from the retention time (t<sub>R</sub>) observed in a fast gradient reverse-phase HPLC.

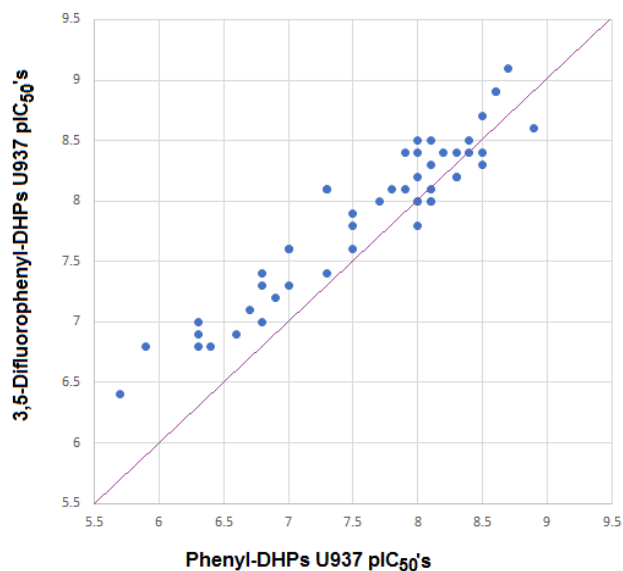


**Figure 6.** Comparison of U937 cellular potencies of phenyl-DHPs compared to their 3,5-difluorophenyl-DHP analogs.

**Table 10. Rat Pharmacokinetic Profiles of DHPs**

IV parameters <sup>a</sup>					PO parameters <sup>b</sup>		
Cpd	Cl (mL/min/Kg)	V <sub>ss</sub> (L/Kg)	t <sub>1/2</sub> (min.)	AUC <sub>0-∞</sub> (μg·h/mL)	C <sub>max</sub> (ng/mL)	T <sub>max</sub> (min.)	F (%)
54	44	1.7	51	0.42	795	30	210 <sup>c</sup>
72	18	1.6	60	0.80			
74	47	6.1	114	0.40	73	38	99
76	46	4.6	99	0.41	215	30	88
77	14	1.3	102	1.3	1100	25	130

<sup>a</sup>IV arm dosed at 1 mg/kg in 5% DMSO/20% Cavitron™ aqueous solution. <sup>b</sup>Oral arm dosed at 2 mg/kg in 5% DMSO/6% Cavitron™ aqueous solution. <sup>c</sup>High bioavailability calculated in a non-crossover fashion using average exposures from separate oral and iv studies.

The FaSSIF solubility of DHP **77** was in a reasonable range of 0.25 mg/mL after 4 h at 37 °C. In addition to good stability in rat and human hepatocytes, inhibitor **77** was also stable in mouse, minipig, dog and monkey hepatocytes with half-lives in the first three over 3 hours, and 92 minutes in the fourth. The pharmacokinetic profile of **77** in mouse, mini-pig and monkey, as detailed in Table 11, showed a similar profile to rat (Table 10) with low clearances, good exposures and good oral bioavailability. DHP **77** displayed a high free fraction in blood in mouse (45%), rat (41%), monkey (55%) and human (47%). Allometric scaling and in vitro to in vivo extrapolations with and without effects of protein binding were used to generate predictions of the human pharmacokinetic parameters of **77** (Table 12). These different methodologies showed a high level of correlation and predicted **77** to have moderate bioavailability, moderate to low clearance with a moderate volume and a terminal half-life in the order of 4 hours in humans. A human whole blood assay in which the necroptosis pathway is activated through stimulation with TNF, co-incubated with the caspase inhibitor zVAD.fmk and the SMAC mimetic RMT 5265,<sup>21</sup> was employed to establish the target concentration. In this assay DHP **77** was also shown to have good potency as



measured by inhibition of cytokine MIP-1 $\alpha$  (IC<sub>50</sub> = 8.5 nM). The average clearance and volume values were then used to reconstruct a mono-exponential predicted human blood concentration time profile. As shown in Figure 7, a dose of 175 mg twice daily is predicted to maintain blood concentrations above the human whole blood inhibition IC<sub>90</sub> level over 24 hours.

**Table 11. IV/PO Pharmacokinetic Profiles of DHP 77**

Species	IV parameters				PO parameters		
	Cl (mL/min/Kg)	t <sub>1/2</sub> (min.)	V <sub>ss</sub> (L/Kg)	AUC <sub>0-∞</sub> (μg·h/mL)	C <sub>max</sub> (ng/mL)	T <sub>max</sub> (min.)	F (%)
Mouse <sup>a</sup>	34	32	1.8	1.1	5414	30	
Minipig <sup>b</sup>	13	78	1.3	1.3	576	80	65
Monkey <sup>b</sup>	5.5	144	1.1	3.1	480	120	40

<sup>a</sup>IV arm dosed at 2 mg/kg in 5% DMSO/20% Cavitron™ aqueous solution. Oral arm dosed at 30 mg/kg in 1% aqueous methylcellulose as a suspension. <sup>b</sup>IV arm dosed at 1 mg/kg in 5% DMSO/20% Cavitron™ aqueous solution. Oral arm dosed at 2 mg/kg in 5% DMSO/6% Cavitron™ aqueous solution.

**Table 12. Average Predicted Human PK Profile of DHP 77 Based on Allometry and In Vitro to In Vivo Extrapolation.**

Parameter	Average	95% C.I. <sup>a</sup>	-95% C.I. <sup>a</sup>
Clearance (mL/min/kg)	7.6	9.1	6.2
Volume (L/kg)	1.3	1.4	1.1
Half life (h) <sup>b</sup>	3.8	4.3	3.3
Bioavailability (%)	74	80	68

<sup>a</sup> The  $\pm$  95% confidence intervals represent variability in parameter estimates from different methodologies. <sup>b</sup>Half-life determined from the terminal phase of the predicted human PK profile

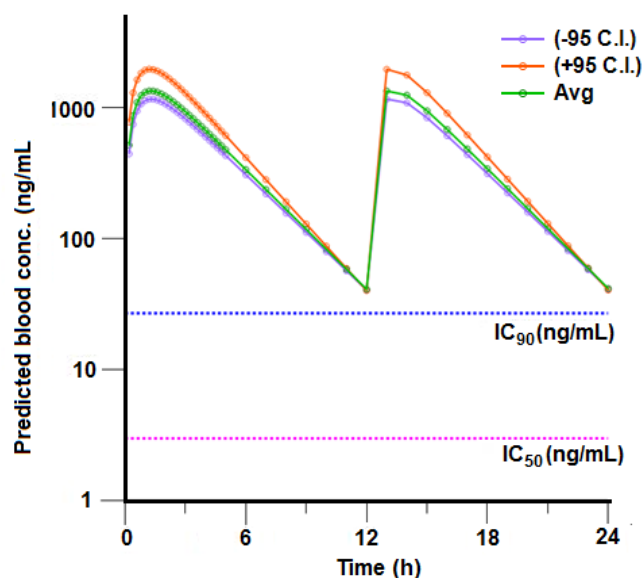


**Figure 7.** Predicted human blood concentration time profile of DHP **77** dosed at 175 mg twice daily overlaid with the human whole blood inhibition  $IC_{90}$  and  $IC_{50}$  concentrations.

To confirm the binding mode, DHP **77** was crystallized in the RIP1 kinase domain which showed it bound to the allosteric region in the back of the ATP pocket similar to the pyrrolidine pivalate **11** (Figure 8a). Although inhibitor **77** does not occupy the same space as the adenine ring of ATP, the piperidine-oxadiazole portion does occupy space where the ATP phosphates would reside and the inhibitor shows competitive inhibition with respect to ATP. The pyrazole carbonyl of **77** accepts a hydrogen bond from the backbone nitrogen of Asp156, with the chair conformation of the piperidine demonstrating a complementary shape to the pocket geometry and providing a vector for the oxadiazole to access the solvation front at the entrance to the active site pocket between Lys45 and Leu157 (Figure 8b).

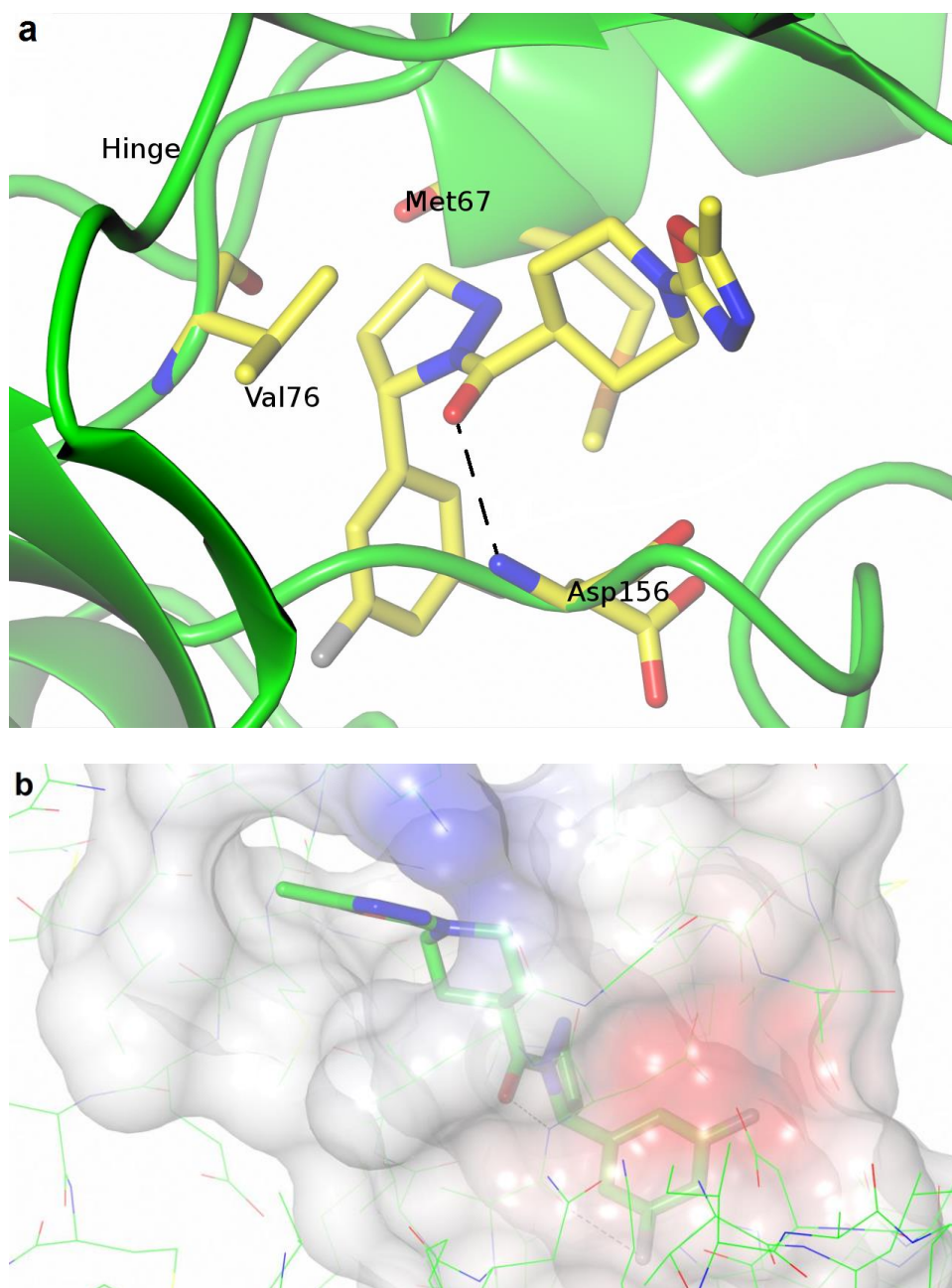


**Figure 8.** (a) Co-crystal structure of RIP1 (1–294, C34A, C127A, C233A, and C240A) and DHP 77. (b) Location of oxadiazole of 77 at the solvation front at the entrance to the active site pocket. Coordinates and structure factors for this cocrystal structure have been deposited in the Protein Data Bank with the accession numbers 6R5F.

A long-standing goal of ours has been to evaluate RIP1 kinase inhibitors in rodent chronic models of disease. This has been hampered by the reduced non-primate RIP1 kinase potency we have observed for all type III inhibitors that target the allosteric pocket of RIP1 kinase. For example, for DHP **77** the cellular potency in prevention of necrotic death in murine fibrosarcoma L929 cells ( $IC_{50} = 3.2 \mu M$ ) represents a 50-fold reduction compared to human U937 cells ( $IC_{50} = 63 \text{ nM}$ ). However, DHP **76** had significantly improved mouse cell L929 cellular efficacy ( $IC_{50} = 32 \text{ nM}$ ). The increased RIP1 kinase murine potency of **76** relative to other DHPs may be due to the cyano-pyrimidine making hydrogen bond interactions with the mouse glycine-rich loop, which is predicted to have less conformational flexibility than the human glycine-rich loop (see Supporting Information). The superior mouse potency of DHP **76** afforded us the opportunity to utilize this RIP1 kinase inhibitor as an in vivo tool compound in murine chronic models of disease. Administration of DHP **76** in mouse chow at doses of 10 and 100 mg/kg/day were able to maintain concentrations above the L929  $IC_{50}$  and  $IC_{90}$ , respectively, over a 24h period (Figure 9). During 6 weeks of dosing at the top dose of 100 mg/kg/day, serum concentrations of **76** were consistently maintained above the L929  $\sim IC_{90}$  and were well tolerated, as shown in figure 10. Another option would be to administer DHP **76** via oral dosing twice daily, but for these chronic studies lasting up to 6 weeks duration food-based delivery was chosen for convenience. A higher dose of 300 mg/kg/day was also evaluated via food-based delivery, but this was not optimal since a decrease in food consumption accompanied by weight loss was observed, presumably because this higher concentration of drug was affecting the food's taste.

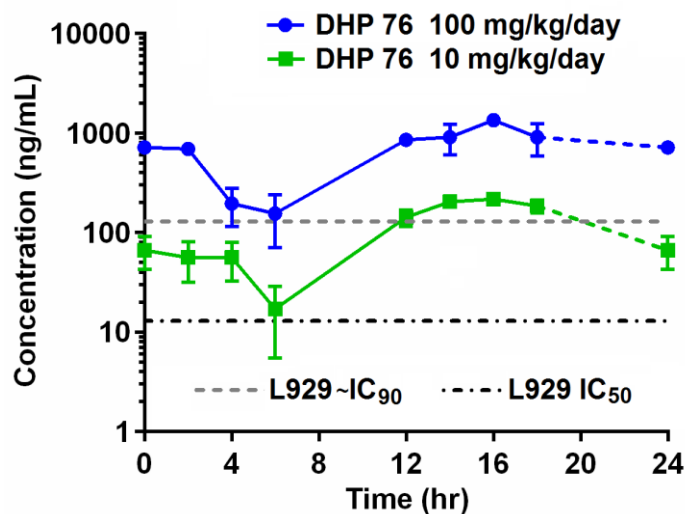


**Figure 9.** DHP 76 dosed in mouse chow maintains concentrations above the murine L929 IC<sub>90</sub> over 24 hours. Concentrations decrease during daytime when mice are least active and feeding less. The 24 hour time point is extrapolated with the assumption that the profile returns to the 0 hour time point level and this is indicated by dotted lines from 18-24 hour timepoints.

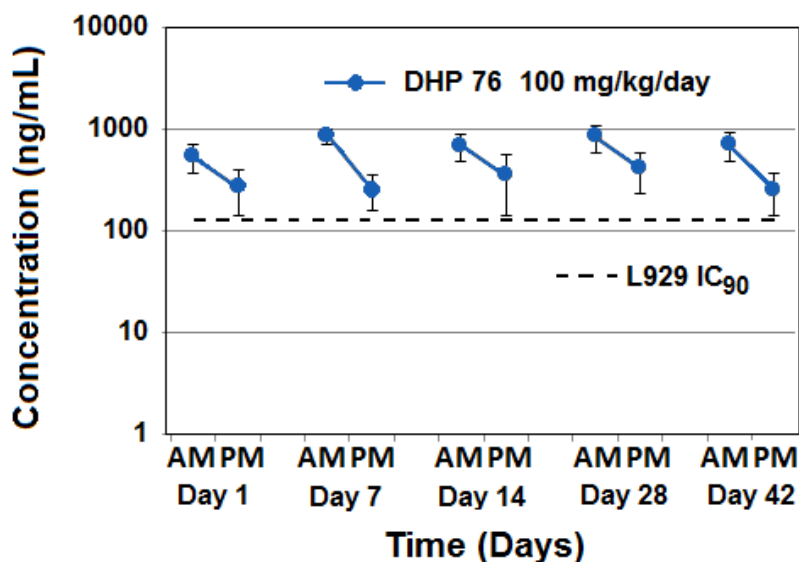


**Figure 10.** DHP **76** dosed in mouse chow maintains concentrations above the murine L929 IC<sub>90</sub> over 24 hours. Sampling was done early morning after nocturnal feeding when drug concentrations should be at their maximum, and late afternoon when concentrations should approach their lowest.

Inhibition of RIP1 kinase has been implicated in protection against the experimental autoimmune encephalomyelitis (EAE) mouse model of human multiple sclerosis.<sup>17,22</sup> To evaluate the efficacy of RIP1 kinase inhibitor **76** in this chronic model we elected to administer the inhibitor via mouse food to maintain serum concentrations above either estimated IC<sub>90</sub> and IC<sub>50</sub> L929 inhibition levels over the course of the study. Mice were pre-dosed with DHP **76** in mouse chow one day prior to EAE induction, such that mice (15 mice per group) received on average 96 mg/kg/day or 9.6 mg/kg/day of **76** in diet, or control diet, as shown in Figure 11. At both of these doses, the concentration of DHP **76** in mouse brain was determined to be close to parity (0.9-1.0) compared to blood levels indicating high murine CNS penetration of this inhibitor. The free fraction of DHP **76** in mouse blood and brain homogenate were 15 and 37%, respectively, leading to a brain-to-blood unbound ratio (K<sub>p,uu</sub>) of 2.5. EAE induction was achieved as described in the supporting information. Mice were monitored daily until 35 days post-induction and scored for clinical signs of disease (see supporting information for details on scoring). DHP **76** showed protection in this EAE model at the dose maintaining concentration over the cellular L929 estimated IC<sub>90</sub> level, exhibiting a delay in the disease onset and reduced clinical severity. The dose group targeting sustained L929 IC<sub>50</sub> inhibition level was not efficacious. This may be useful when considering doses in future clinical trials. The efficacy of DHP **76** in this EAE model is comparable to that observed by Yoshikawa et al. with benzoxazepinone **5** over a shorter dosing duration of 26 days.<sup>17</sup>

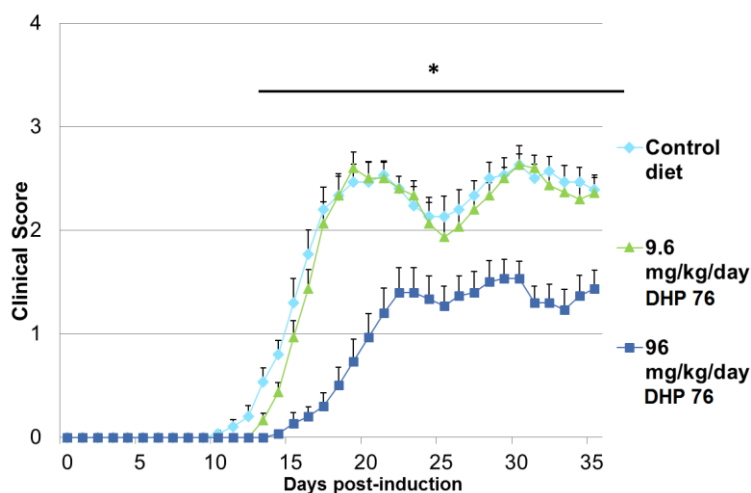


**Figure 11.** Assessment of DHP **76** in the mouse EAE model of human multiple sclerosis over 5 weeks. DHP **76** was dosed in diet at either 9.6 or 96 mg/kg/day, to maintain concentrations above the murine L929 IC<sub>50</sub> or IC<sub>90</sub>, respectively. Mice were scored for clinical signs of disease (see supporting information). Data are presented as mean  $\pm$  SEM. Statistical significances: \*  $p < 0.05$ , control versus 9.6 mg/kg/day during days 12-14, control versus 96 mg/kg/day starting from day 12 and continued until day 35 (one-way ANOVA).

Inhibition of RIP1 kinase by food-based dosing of DHP **76** was also evaluated in a Rd10 mouse model of human retinitis pigmentosa (RP). Rd10 mice have a mutation in the rod-specific gene that encodes rod cGMP phosphodiesterase  $\beta$ -subunit.<sup>23</sup> Mice were dark reared to 30 days old, at which point they were moved to a 12-hour light/dark cycle to induce retinal degeneration. Mice were pre-dosed with DHP **76** in food-based dosing two days prior to the switch to normal cyclic light, such that mice (15 per group) received on average 100 mg/kg/day of **76** in diet or control diet. Protection of retinal cell function was demonstrated by electroretinography (ERG) recordings of mice aged 39 and 46 days old, as shown in Figure 12. Scotopic measurements are representative

of rod signaling and photopic measurements are representative of cone signaling. In addition, protection in retinal cell survival was confirmed by measurement of the thickness of the Outer Nuclear Cell (ONL) layers in H&E stained retinal tissue sections collected at P46 (see supporting information).

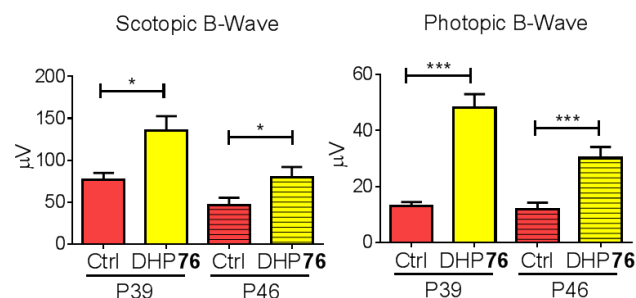


**Figure 12.** Assessment of DHP 76 in the mouse Rd model of human Retinitis Pigmentosa up to 46 days old. DHP 76 was dosed in diet at 100 mg/kg/day, to maintain concentrations above the murine L929 IC<sub>90</sub>. Mice retinal cell function was measured at post-natal days P39 and P46 by ERG. Mice on DHP 76 diet displayed significantly higher ERG amplitudes at both P39 and P46 compared to mice on control diet (\*,  $p < 0.05$  for scotopic b-wave, and \*\*\*,  $p < 0.001$  for photopic b-wave; Mann-Whitney t-test).

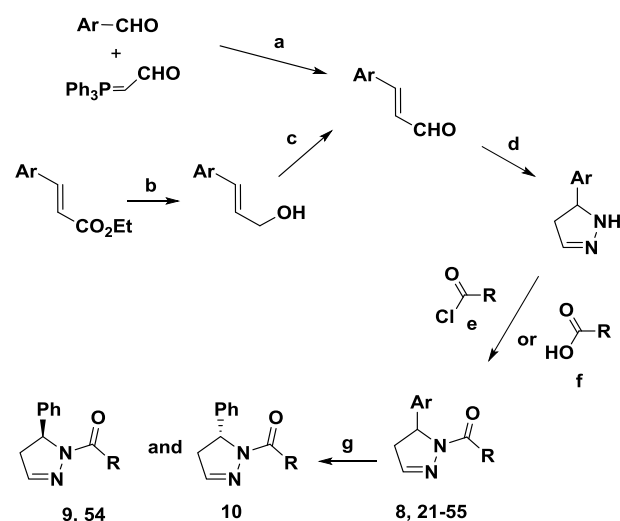
## CHEMISTRY

The synthetic route to prepare dihydropyrazole **8-10** and **21-55** is summarized in Scheme 1. The required aryl  $\alpha,\beta$ -unsaturated aldehyde is obtained either by Wittig reaction of the aryl aldehyde or from the aryl  $\alpha,\beta$ -unsaturated ester via DIBAL-H reduction to the alcohol, followed by oxidation with manganese dioxide. The aryl  $\alpha,\beta$ -unsaturated aldehyde is cyclized to the dihydropyrazole with hydrazine, which is subsequently acylated with an acid chloride or coupled



with a carboxylic acid. The active (*S*)-enantiomer dihydropyrazoles **9** and **54** were isolated from their racemates via chiral HPLC separation.

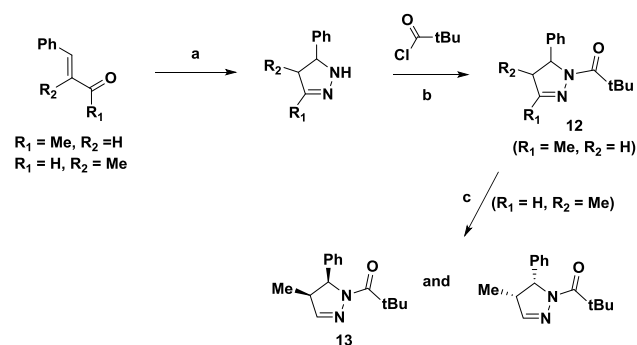
### Scheme 1 Generic Synthesis of DHPs 8-10 and 21-55



Reagent and conditions: (a) THF, 80 °C; (b) DIBAL-H, toluene; (c) MnO<sub>2</sub>, DCM; (d) hydrazine, tBuOH, 80 °C; (e) DIPEA, DCM; (f) HATU, DIPEA, DMSO; (g) chiral chromatography

The 3- and 4-methyl substituted dihydropyrazole **12** and **13** were prepared from hydrazine cyclization of either (E)-4-phenylbut-3-en-2-one or (E)-2-methyl-3-phenylacrylaldehyde, followed by acylation with pivaloyl chloride (Scheme 2). The cyclization with (E)-2-methyl-3-phenylacrylaldehyde yields predominantly the *cis* diastereoisomer, from which the active (4*S*,5*S*)-enantiomer **13** was isolated via chiral HPLC separation.

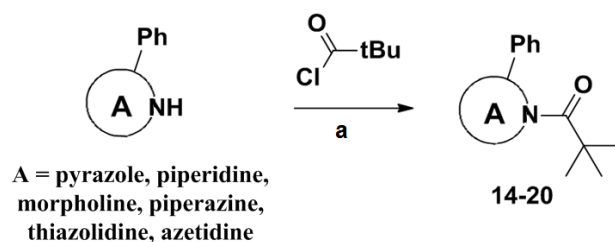
### Scheme 2. Synthesis of DHPs 12 and 13.



Reagent and conditions: (a) hydrazine, tBuOH, 80 °C; (b) DIPEA, DCM; (c) chiral chromatography

The phenyl substituted pyrazole, piperidine, morpholine, piperazine, thiazolidine and azetidine heterocycles could be acylated directly with pivaloyl chloride (Scheme 3).

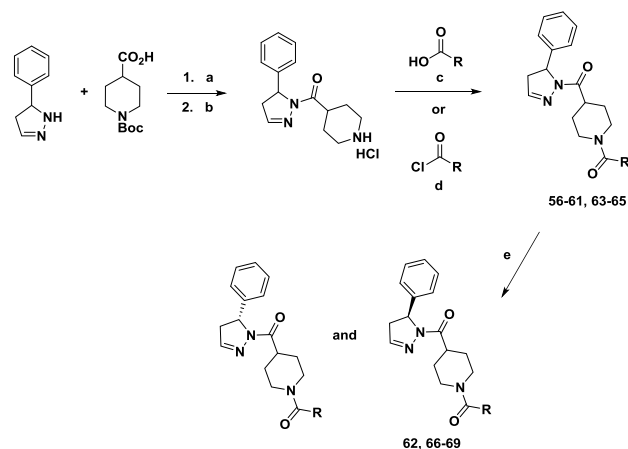
### Scheme 3. Synthesis of DHPs 14-20.



Reagent and conditions: (a) DIPEA, DCM

For the preparation of N-acylpiperidine DHPs **56-69**, coupling of 5-phenyl-4,5-dihydro-1H-pyrazole with N-BOC-piperidine-4-carboxylic acid followed by deprotection yielded the common intermediate (5-phenyl-4,5-dihydro-1H-pyrazol-1-yl)(piperidin-4-yl)methanone. This was subsequently acylated with an acid chloride or coupled with a carboxylic acid. The active (*S*)-enantiomer dihydropyrazoles **62** and **66-69** were isolated from their racemates via chiral HPLC separation (Scheme 4).

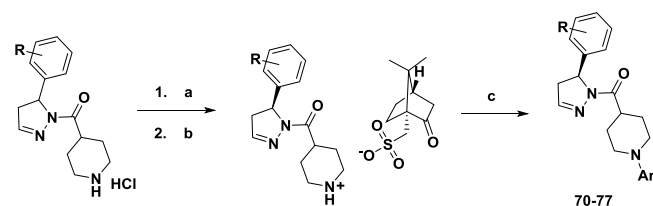
#### Scheme 4. Synthesis of DHPs 56-69.



Reagent and conditions: (a) HATU, DIPEA, DMF; (b) HCl, DCM; (c) T<sub>3</sub>P or HATU, DIPEA, DCM or 2-Me-THF; (d) DIPEA, DCM; (e) chiral chromatography

For the preparation of N-arylpiperidine DHPs, the common intermediate (5-phenyl-4,5-dihydro-1H-pyrazol-1-yl)(piperidin-4-yl)methanone was first resolved via a diastereoselective crystallization of its (1*R*)-(-)-10-camphorsulfonic acid salt in ethanol. This was subsequently subjected to N-arylation to yield the active (*S*)-enantiomer N-arylpiperidine DHPs **70-77** (Scheme 5).

#### Scheme 5. Synthesis of DHPs 70-77.



Reagent and conditions: (a) NaOH; (b) (1*R*)-(-)-10-Camphorsulfonic acid, EtOH crystallization; (c) Ar-Cl, DIPEA, MeCN

## CONCLUSIONS

We have described the identification of a highly potent and selective dihydropyrazole RIP1 kinase inhibitor lead **9** discovered by optimization of two high throughput screening hits. Through understanding of the SAR and focusing on lowering lipophilicity and reducing intrinsic clearances led to discovery of DHP **77** with a favorable pharmacokinetic profile in multiple species and good predicted human exposure. In addition, we identified DHP **76** with potent RIP1 kinase murine activity as an in vivo tool compound. DHP **76** demonstrated efficacy in chronic mouse models of both multiple sclerosis (EAE) and retinitis pigmentosa (Rd10). Further details on the progression of RIP1 inhibitors from this series will be disclosed in due course.

## EXPERIMENTAL

### General Methods.

Unless otherwise noted, starting materials and reagents were purchased from commercial sources and used without further purification. N-(3-Chlorophenyl)-5-phenyl-4,5-dihydro-1H-pyrazole-1-carboxamide (**6**), 2,2-dimethyl-1-(2-phenylpyrrolidin-1-yl)propan-1-one (**7**) and 1-(2,2-dimethylpropanoyl)-2-(3-fluorophenyl)pyrrolidine (**11**) are commercially available building blocks. Air or moisture sensitive reactions were carried out under a nitrogen atmosphere. Anhydrous solvents were obtained from Sigma-Aldrich. Microwave irradiation was carried out in a Personal Chemistry Emrys Optimizer microwave. Silica gel chromatography was performed using standard techniques or using silica gel cartridges (RediSep normal phase disposable flash columns) on an Isco CombiFlash. Reverse phase HPLC purification was conducted on a Gilson HPLC (monitoring at a wavelength of 214 or 254 nm) with a YMC ODS-A C18 column (5  $\mu$ m, 75 mm 30 mm), eluting with 5-90% CH<sub>3</sub>CN in H<sub>2</sub>O with 0.1% TFA unless otherwise noted. <sup>1</sup>H NMR spectra were recorded on a Bruker Advance or Varian Unity 400MHz spectrometer as

solutions in DMSO- $d_6$  (unless otherwise stated). Chemical shifts ( $\delta$ ) are reported in ppm relative to an internal solvent reference. Apparent peak multiplicities are described as s (singlet), br s (broad singlet), d (doublet), dd (doublet of doublets), t (triplet), q (quartet), or m (multiplet). Coupling constants ( $J$ ) are reported in hertz (Hz) after the integration. All tested compounds were determined to be >95% purity by LCMS or HPLC unless otherwise noted.

**2,2-Dimethyl-1-(5-phenyl-4,5-dihydro-1H-pyrazol-1-yl)propan-1-one (8).** Hydrazine (6.84 mL, 190 mmol) was heated to reflux. A solution of cinnamaldehyde (10 g, 76 mmol) in *tert*-butanol (20 mL) was added dropwise and the mixture was refluxed overnight. The reaction mixture was concentrated under reduced pressure. The crude material was then diluted with DCM and washed with water. The combined organic layers were washed with water and then dried over sodium sulfate, filtered and concentrated under reduced pressure to provide 5-phenyl-4,5-dihydro-1H-pyrazole (9.4 g, 64.3 mmol, 85 % yield) of a yellow oil. The product was carried onto the next reaction without further purification. MS ( $m/z$ ) 147 ( $M+H^+$ ).

To a solution of 5-phenyl-4,5-dihydro-1H-pyrazole (150 mg, 1.026 mmol) in DCM (3 mL) was added DIPEA (0.376 mL, 2.155 mmol) followed by pivaloyl chloride (0.153 mL, 1.129 mmol). The reaction was very exothermic. After 15 minutes LC/MS showed the reaction was complete. The reaction was concentrated and then taken up in DMSO and purified by reverse phase preparative HPLC to provide pure 2,2-dimethyl-1-(5-phenyl-4,5-dihydro-1H-pyrazol-1-yl)propan-1-one (**8**) (188 mg, 53 % yield).  $^1H$  NMR (400 MHz, DMSO- $d_6$ )  $\delta$  ppm 1.25 (s, 9 H), 2.55 (ddd,  $J=18.7, 4.6, 1.8$  Hz, 1 H), 3.37 (ddd,  $J=18.8, 11.9, 1.6$  Hz, 1 H), 5.31 (dd,  $J=11.9, 4.6$  Hz, 1 H), 7.05 - 7.12 (m, 2 H), 7.18 (t,  $J=1.6$  Hz, 1 H), 7.20 - 7.25 (m, 1 H), 7.28 - 7.34 (m, 2 H). MS ( $m/z$ ) 231 ( $M+H^+$ ).

(*S*)-2,2-Dimethyl-1-(5-phenyl-4,5-dihydro-1H-pyrazol-1-yl)propan-1-one (9) and (*R*)-2,2-dimethyl-1-(5-phenyl-4,5-dihydro-1H-pyrazol-1-yl)propan-1-one (10). 2,2-Dimethyl-1-(5-phenyl-4,5-dihydro-1H-pyrazol-1-yl)propan-1-one (188 mg, 0.546 mmol) was separated into its 2 enantiomers via chiral chromatography preparative HPLC (IC column, 20 x 250mm, flow rate: 20 mL/min, 10:90 EtOH:heptane). Obtained were (*S*)-2,2-dimethyl-1-(5-phenyl-4,5-dihydro-1H-pyrazol-1-yl)propan-1-one (9) (74 mg, 40% yield),  $[\alpha]_D = -157^\circ$  (conc = 0.110, MeOH), ee = 100%,  $^1\text{H NMR}$  (DMSO- $d_6$ )  $\delta$ : 1.26 (s, 9H), 2.56 (ddd,  $J=18.8, 4.5, 1.8$  Hz, 1H), 3.38 (ddd,  $J=18.9, 11.9, 1.5$  Hz, 1H), 5.32 (dd,  $J=11.9, 4.5$  Hz, 1H), 7.04 - 7.12 (m, 1H), 7.16 - 7.27 (m, 1H), 7.28 - 7.36 (m, 1H), MS ( $m/z$ ) 231 ( $M+H^+$ ) and (*R*)-2,2-dimethyl-1-(5-phenyl-4,5-dihydro-1H-pyrazol-1-yl)propan-1-one (10) (78 mg, 41% yield),  $[\alpha]_D = +162^\circ$  (conc = 0.106, MeOH), ee = 100%. The absolute configurations of the enantiomer were determined by ab initio VCD analysis.

**2,2-Dimethyl-1-(3-methyl-5-phenyl-4,5-dihydro-1H-pyrazol-1-yl)propan-1-one (12).** Hydrazine hydrate (2.6 mL, 82.2 mmol) was dissolved in Et<sub>2</sub>O (15 mL) and the solution cooled to 0 °C in an ice bath. (E)-4-Phenylbut-3-en-2-one (1 g, 6.85 mmol) dissolved in Et<sub>2</sub>O (10 mL) was slowly added and the reaction mixture stirred for 18 h, during which time the reaction mixture warmed to rt. The reaction mixture was then concentrated in vacuo and partitioned between DCM (100 mL) and water (100 mL), the aqueous phase was separated and extracted with additional DCM (100 mL), the combined organic fractions were then concentrated in vacuo to give 3-methyl-5-phenyl-4,5-dihydro-1H-pyrazole (1.15 g) as a yellow oil, MS ( $m/z$ ) 147 ( $M+H^+$ ) 161.

To a solution of 3-methyl-5-phenyl-4,5-dihydro-1H-pyrazole (0.110 g, 0.687 mmol) and triethylamine (0.105 mL, 0.755 mmol) in DCM (2.5 mL) was added pivaloyl chloride (0.085 mL, 0.687 mmol) dropwise neat. The reaction was allowed to stir at rt for 15 min. Analysis of the crude reaction by LCMS confirmed the formation of the desired product. The reaction was concentrated

and the residue purified by reverse phase preparative HPLC [40-70% acetonitrile:water (0.1% NH<sub>4</sub>OH modifier), C18 50x30 mm Gemini column, flow rate 47 mL/min] to give 2,2-dimethyl-1-(3-methyl-5-phenyl-4,5-dihydro-1H-pyrazol-1-yl)propan-1-one (**12**) (44 mg, 26% yield) as a light yellow viscous oil. <sup>1</sup>H NMR (400 MHz, CDCl<sub>3</sub>) δ ppm 1.33 (s, 9 H), 2.05 (s, 3 H), 2.49 - 2.58 (m, 1 H), 3.17 - 3.28 (m, 1 H), 5.43 (dd, *J*=11.8, 4.6 Hz, 1 H), 7.09 - 7.17 (m, 2 H), 7.18 - 7.33 (m, 3 H). MS (m/z) 245 (M+H<sup>+</sup>).

**2,2-Dimethyl-1-((4*S*,5*S*)-4-methyl-5-phenyl-4,5-dihydro-1H-pyrazol-1-yl)propan-1-one (**13**).** (E)-2-Methyl-3-phenylacrylaldehyde (2.0 g, 13.67 mmol) and hydrazine hydrate (6.84 g, 136.7 mmol) were dissolved in *tert*-butanol (20 mL) and heated to reflux for 36 h. The reaction mixture was concentrated under reduced pressure. The crude material was then diluted with DCM and washed with 5% sodium bicarbonate solution (20 mL). The organic phase was filtered and concentrated under reduced pressure to provide the crude product which was purified by silica gel chromatography (eluting with cyclohexanes plus EtOAc from 40-100%) to yield 4-methyl-5-phenyl-4,5-dihydro-1H-pyrazole (1.1 g, 50% yield) as a mixture of diastereoisomers.

To a solution of 4-methyl-5-phenyl-4,5-dihydro-1H-pyrazole (600 mg, 3.74 mmol) in dichloromethane (DCM) (6 mL) was added DIPEA (1.3 mL, 7.48 mmol) followed by pivaloyl chloride (542 mg, 4.49 mmol). The reaction was stirred overnight at rt under nitrogen. The reaction was quenched in water (10 mL) and extracted with DCM (20 mL). The organic phase was separated and concentrated to yield the crude product (1.2 g) as a yellow oil. Reverse phase preparative HPLC purification yielded both *cis*-2,2-dimethyl-1-(4-methyl-5-phenyl-4,5-dihydro-1H-pyrazol-1-yl)propan-1-one (141.8 mg, 16% yield), <sup>1</sup>H NMR (500 MHz, DMSO-*d*<sub>6</sub>) δ ppm 0.60 (d, *J*=7.57 Hz, 3 H), 1.26 (s, 9 H), 3.48 - 3.61 (m, 1 H), 5.37 (d, *J*=11.51 Hz, 1 H), 6.98 (d, *J*=7.41 Hz, 2H), 7.03 (s, 1 H), 7.20 - 7.25 (m, 1 H), 7.28 - 7.34 (m, 2 H), MS (m/z) 245 (M+H<sup>+</sup>)

and trans-2,2-dimethyl-1-(4-methyl-5-phenyl-4,5-dihydro-1H-pyrazol-1-yl)propan-1-one (39.8 mg, 4% yield),  $^1\text{H}$  NMR (500 MHz, DMSO- $d_6$ )  $\delta$  ppm 1.19 (d,  $J=7.25$  Hz, 3 H), 1.26 (s, 9 H) 2.75 - 2.83 (m, 1 H) 4.83 (d,  $J=4.26$  Hz, 1 H) 7.09 (d,  $J=7.57$  Hz, 2 H) 7.12 (s, 1 H) 7.23 (t,  $J=7.25$  Hz, 1 H) 7.31 (t,  $J=7.25$  Hz, 2 H), MS (m/z) 245 ( $\text{M}+\text{H}^+$ ).

Cis-2,2-dimethyl-1-(4-methyl-5-phenyl-4,5-dihydro-1H-pyrazol-1-yl)propan-1-one (128 mg, 0.52 mmol) was separated into its 2 enantiomers via chiral chromatography on reverse phase HPLC (IC column, 20 x 250mm, flow rate: 20 mL/min, 10:90 EtOH:Heptane). Obtained was 2,2-dimethyl-1-((4*S*,5*S*)-4-methyl-5-phenyl-4,5-dihydro-1H-pyrazol-1-yl)propan-1-one (**13**) (24 mg, 19% yield),  $[\alpha]_D = -330^\circ$  (conc = 0.15, MeOH), ee = >99.5%,  $^1\text{H}$  NMR (400 MHz, DMSO- $d_6$ )  $\delta$  ppm 0.60 (d,  $J=7.58$  Hz, 3 H) 1.26 (s, 9 H) 3.47-3.64 (m, 1 H) 5.37 (d,  $J=11.37$ , Hz, 1 H) 6.99 (d,  $J=7.07$  Hz, 2 H) 7.04 (d,  $J=1.26$  Hz, 1 H) 7.19-7.27 (m, 1 H) 7.27 - 7.37 (m, 2 H). Also obtained was 2,2-dimethyl-1-((4*R*,5*R*)-4-methyl-5-phenyl-4,5-dihydro-1H-pyrazol-1-yl)propan-1-one (25 mg, 20% yield),  $[\alpha]_D = +334^\circ$  (conc = 0.23, MeOH), ee = >99.5%,  $^1\text{H}$  NMR (400 MHz, DMSO- $d_6$ )  $\delta$  ppm 0.60 (d,  $J=7.58$  Hz, 3 H) 1.26 (s, 9 H) 3.47-3.64 (m, 1 H) 5.37 (d,  $J=11.37$ , Hz, 1 H) 6.99 (d,  $J=7.07$  Hz, 2 H) 7.04 (d,  $J=1.26$  Hz, 1 H) 7.19-7.27 (m, 1 H) 7.27 - 7.37 (m, 2 H). The absolute confirmation was assigned based on the RIP1 kinase active enantiomer **13**, by comparison to **9** having the (5*S*) configuration.

**(1-Methylpiperidin-4-yl)(5-phenyl-4,5-dihydro-1H-pyrazol-1-yl)methanone (53).** To a solution of 5-phenyl-4,5-dihydro-1H-pyrazole (250 mg, 1.71 mmol) in DCM (10 mL) was added DIPEA (0.627 mL, 3.59 mmol), followed by 1-acetylpiperidine-4-carbonyl chloride (357 mg, 1.88 mmol). The reaction was stirred at rt for 14 h. The reaction was quenched in water (25 mL) and extracted with DCM (2 x 25 mL). The combined organic fractions were washed with saturated sodium bicarbonate solution (20 mL). The organic phase was dried over sodium sulfate, filtered



and concentrated under reduced pressure to provide the crude product, which was purified by silica gel chromatography (eluting with 15% EtOAc in hexanes) to yield 1-(4-(5-phenyl-4,5-dihydro-1H-pyrazole-1-carbonyl)piperidin-1-yl)ethanone (**53**) (180 mg, 35% yield). <sup>1</sup>H NMR (400 MHz, DMSO-d<sub>6</sub>) δ ppm 1.30 - 1.59 (m, 2 H) 1.73 (t, *J*=11.29 Hz, 1 H) 1.79 - 1.94 (m, 1 H) 2.00 (s, 3 H) 2.59 - 2.82 (m, 2 H) 3.02 - 3.22 (m, 1 H) 3.24 - 3.43 (m, 1 H) 3.51 (dd, *J*=17.87, 11.95 Hz, 1 H) 3.84 (d, *J*=13.59 Hz, 1 H) 4.36 (br. s., 1 H) 5.33 (dd, *J*=11.84, 4.60 Hz, 1 H) 7.13 (d, *J*=7.67 Hz, 2 H) 7.19 - 7.29 (m, 2 H) 7.29 - 7.39 (m, 2 H), MS (*m/z*) 300 (*M*+*H*<sup>+</sup>).

**(*S*)-(1-Methylpiperidin-4-yl)(5-phenyl-4,5-dihydro-1H-pyrazol-1-yl)methanone (**54**).** 1-(4-(5-Phenyl-4,5-dihydro-1H-pyrazole-1-carbonyl)piperidin-1-yl)ethanone (50 mg, 0.167 mmol) was separated into its 2 enantiomers via chiral chromatography preparative HPLC (column: 30mm x 25cm Chiralpak AD-H, flow rate: 30 mL/min, 1:1 EtOH/Heptane). Obtained was (*S*)-1-(4-(5-phenyl-4,5-dihydro-1H-pyrazole-1-carbonyl)piperidin-1-yl)ethanone (**54**) (24 mg, 48% yield), [*α*]<sub>D</sub> = -120° (conc = 0.377, MeOH), ee = >99%, <sup>1</sup>H NMR (400 MHz, DMSO-d<sub>6</sub>) δ ppm 1.19 - 1.63 (m, 2 H) 1.70 (t, *J*=11.00 Hz, 1 H) 1.79 - 1.88 (m, 1 H) 1.98 (s, 3 H) 2.56 - 2.75 (m, 2 H) 3.05 - 3.16 (m, 1 H) 3.22 - 3.38 (m, 1 H) 3.38 - 3.58 (m, 1 H) 3.82 (d, *J*=13.69 Hz, 1 H) 4.25 - 4.41 (m, 1 H) 5.31 (dd, *J*=11.98, 4.65 Hz, 1 H) 7.05 - 7.14 (m, 2 H) 7.17 - 7.28 (m, 2 H) 7.28 - 7.37 (m, 2 H), MS (*m/z*) 300 (*M*+*H*<sup>+</sup>). Also obtained was (*R*)-1-(4-(5-phenyl-4,5-dihydro-1H-pyrazole-1-carbonyl)piperidin-1-yl)ethanone (24 mg, 48% yield [*α*]<sub>D</sub> = +135° (conc = 0.1781, MeOH), ee = >99%. <sup>1</sup>H NMR (400 MHz, DMSO-d<sub>6</sub>) δ ppm 1.23 - 1.56 (m, 2 H) 1.64 - 1.77 (m, 1 H) 1.77 - 1.87 (m, 1 H) 1.98 (s, 3 H) 2.56 - 2.75 (m, 2 H) 3.03 - 3.17 (m, 1 H) 3.23 - 3.37 (m, 1 H) 3.39 - 3.57 (m, 1 H) 3.82 (d, *J*=13.69 Hz, 1 H) 4.28 - 4.42 (m, 1 H) 5.31 (dd, *J*=11.98, 4.65 Hz, 1 H) 7.06 - 7.15 (m, 2 H) 7.18 - 7.28 (m, 2 H) 7.28 - 7.37 (m, 2 H), MS (*m/z*) 300 (*M*+*H*<sup>+</sup>). The absolute configurations of the enantiomers were assigned by their RIP1 kinase activity, since the (*S*)-

enantiomer determined for (S)-2,2-dimethyl-1-(5-phenyl-4,5-dihydro-1H-pyrazol-1-yl)propan-1-one (**9**) was known to be the active isomer.

**(S)-6-(4-(5-(3,5-difluorophenyl)-4,5-dihydro-1H-pyrazole-1-carbonyl)piperidin-1-yl)pyrimidine-4-carbonitrile (76).** 1-(*Tert*-butoxycarbonyl)piperidine-4-carboxylic acid (25.2 g, 110 mmol) was dissolved in DCM (300 mL) and PyBroP (53.7 g, 115 mmol) and DIPEA (21.09 mL, 121 mmol) were added and the reaction stirred for 5 min. 5-(3,5-Difluorophenyl)-4,5-dihydro-1H-pyrazole (20 g, 110 mmol) was added and the reaction is stirred for a further 5 h. The solvent was removed under vacuum. The residue was purified by column chromatography (eluting with cyclohexanes plus 3:1 EtOAc/EtOH from 0-50%) to afford the expected product as a yellow oil. This was dissolved in DCM (500mL) and 3M HCl in CPME (91 mL, 274 mmol) was added. The reaction is stirred at rt for 24 h and the precipitate filtered off, washed with DCM (2 x 150mL) and iPr<sub>2</sub>O (3 x 200mL) to give (5-(3,5-difluorophenyl)-4,5-dihydro-1H-pyrazol-1-yl)(piperidin-4-yl)methanone hydrochloride (20g, 55 % yield) as a cream powder. MS (m/z) 294 (M+H<sup>+</sup>).

To a solution of (5-(3,5-difluorophenyl)-4,5-dihydro-1H-pyrazol-1-yl)(piperidin-4-yl)methanone, hydrochloride (20g, 60.6 mmol) in EtOH (50mL) was added 1N sodium hydroxide (79 mL, 79 mmol) solution. The solution was stirred at room temperature for 30 min and then evaporated in vacuo. The crude was extracted with DCM (3 x 150mL). The combined organic extracts were filtered and the filtrate was evaporated under reduced pressure to give the free base as an oil (17.3g, 97% yield). This was dissolved in EtOH (50 mL) and ((1*R*,4*S*)-7,7-dimethyl-2-oxobicyclo[2.2.1]heptan-1-yl)metha((1*R*,4*S*)-7,7-dimethyl-2-oxobicyclo[2.2.1]heptan-1-yl)methanesulfonic acid (14.1 g, 60.6 mmol) was added and the resulting suspension heated at 60 °C for 30 min. The solution was then evaporated to dryness and the partially crystalline crude solid was suspended in EtOH (50 mL) to fully convert it to a crystalline solid, and this suspension was

1  
2  
3 evaporated to dryness to give a light orange crystalline solid. Recrystallisation from hot EtOH  
4 (300mL) gave (S)-(5-(3,5-difluorophenyl)-4,5-dihydro-1H-pyrazol-1-yl)(piperidin-4-  
5  
6 yl)methanone,((1*R*,4*S*)-7,7-dimethyl-2-oxobicyclo[2.2.1]heptan-1-yl)methanesulfonate salt (7g,  
7  
8 22 % yield) as a white powder. Chiral purity of >99% ee was determined by chiral HPLC (Chiralcel  
9  
10 OJ-H column: 4.6 x 150mm, flow rate: 1 mL/min, 1:1 EtOH/Heptane, modifier: 0.1%  
11  
12 diethylamine). <sup>1</sup>H NMR (400 MHz, DMSO-d<sub>6</sub>) δ ppm 0.75 (s, 3 H) 1.05 (s, 3 H) 1.19 - 1.38 (m,  
13  
14 2 H) 1.61 - 1.91 (m, 5 H) 1.91 - 2.10 (m, 2 H) 2.24 (dt, *J*=18.08, 3.87 Hz, 1 H) 2.38 (d, *J*=14.61  
15  
16 Hz, 1 H) 2.60 - 2.83 (m, 2 H) 2.88 (d, *J*=14.61 Hz, 1 H) 2.99 (t, *J*=12.15 Hz, 2 H) 3.28 (br. s., 1  
17  
18 H) 3.31 - 3.42 (m, 1 H) 3.42 - 3.58 (m, 1 H) 5.34 (dd, *J*=11.96, 4.93 Hz, 1 H) 6.85 (d, *J*=6.26 Hz,  
19  
20 2 H) 7.14 (tt, *J*=9.32, 2.25 Hz, 1 H) 7.27 (s, 1 H) 8.29 (br. s., 1 H) 8.55 (br. s., 1 H). MS (m/z) 294  
21  
22 (M+H<sup>+</sup>).  
23  
24  
25  
26  
27

28  
29 To a suspension of (S)-(5-phenyl-4,5-dihydro-1H-pyrazol-1-yl)(piperidin-4-yl)methanone (300  
30  
31 mg, 0.571 mmol) and 6-chloropyrimidine-4-carbonitrile (80 mg, 0.571 mmol) in MeCN (30 mL)  
32  
33 stirred at rt was added DIPEA (184 mg, 1.43 mmol). The reaction vessel was sealed and heated  
34  
35 with stirring to 80 °C for 2 h. The reaction was then evaporated *in vacuo* to give a crude residue  
36  
37 which was purified by column chromatography (eluting with cyclohexanes plus 3:1 EtOAc/EtOH  
38  
39 from 0-30%). Trituration from diisopropyl ether afforded (S)-6-(4-(5-(3,5-difluorophenyl)-4,5-  
40  
41 dihydro-1H-pyrazole-1-carbonyl)piperidin-1-yl)pyrimidine-4-carbonitrile (**76**) (130 mg, 58 %  
42  
43 yield) as a light yellow powder. <sup>1</sup>H NMR (400 MHz, DMSO-d<sub>6</sub>) δ ppm 1.36 - 1.60 (m, 2 H) 1.81  
44  
45 (d, *J*=11.39 Hz, 1 H) 1.95 (d, *J*=11.20 Hz, 1 H) 2.75 (ddd, *J*=19.03, 4.89, 1.52 Hz, 1 H) 3.13 (br.  
46  
47 s., 2 H) 3.36 - 3.55 (m, 2 H) 4.42 (br s, 2H), 5.34 (dd, *J*=11.96, 4.93 Hz, 1 H) 6.84 (d, *J*=6.45 Hz,  
48  
49 2 H) 7.05 - 7.20 (m, 1 H) 7.26 (s, 1 H) 7.57 (s, 1 H) 8.54 (s, 1 H). MS (m/z) 397 (M+H<sup>+</sup>). The  
50  
51 absolute configuration of the enantiomer was confirmed by its RIP1 kinase activity, since the (S)-  
52  
53  
54  
55  
56  
57  
58  
59  
60

enantiomer determined for (*S*)-2,2-dimethyl-1-(5-phenyl-4,5-dihydro-1H-pyrazol-1-yl)propan-1-one (**9**) was known to be the active isomer.

**(*S*)-(5-(3,5-Difluorophenyl)-4,5-dihydro-1H-pyrazol-1-yl)(1-(5-methyl-1,3,4-oxadiazol-2-yl)piperidin-4-yl)methanone (**77**)**. Prepared from (*S*)-(5-(3,5-difluorophenyl)-4,5-dihydro-1H-pyrazol-1-yl)(piperidin-4-yl)methanone, ((1*R*,4*S*)-7,7-dimethyl-2-oxobicyclo[2.2.1]heptan-1-yl)methanesulfonate salt (350 mg, 0.666 mmol), DIPEA (215 mg, 1.67 mmol), and 2-bromo-5-methyl-1,3,4-oxadiazole (109 mg, 0.67 mmol) by the same procedure outline for **76**, except with a reaction temperature of 120 °C. The residue was purified by column chromatography (eluting with DCM plus MeOH from 0-5%) to afford the expected product. Trituration in Et<sub>2</sub>O afforded ((*S*)-(5-(3,5-difluorophenyl)-4,5-dihydro-1H-pyrazol-1-yl)(1-(5-methyl-1,3,4-oxadiazol-2-yl)piperidin-4-yl)methanone (110 mg, 44 % yield) (**77**) as a white foam. <sup>1</sup>H NMR (400 MHz, DMSO-*d*<sub>6</sub>) δ ppm 1.41 - 1.70 (m, 2 H) 1.77 (d, *J*=11.77 Hz, 1 H) 1.91 (d, *J*=11.77 Hz, 1 H) 2.32 (s, 3 H) 2.75 (ddd, *J*=19.03, 4.98, 1.61 Hz, 1 H) 2.98 - 3.16 (m, 2 H) 3.23 - 3.32 (m, 1 H) 3.48 (ddd, *J*=19.03, 12.00, 1.23 Hz, 1 H) 3.81 (d, *J*=12.91 Hz, 2 H) 5.34 (dd, *J*=11.96, 4.93 Hz, 1 H) 6.75 - 6.92 (m, 2 H) 7.12 (tt, *J*=9.35, 2.14 Hz, 1 H) 7.25 (s, 1 H). MS (*m/z*) 376 (*M*+*H*<sup>+</sup>). The absolute configuration of the enantiomer was confirmed by its RIP1 kinase activity, since the (*S*)-enantiomer determined for (*S*)-2,2-dimethyl-1-(5-phenyl-4,5-dihydro-1H-pyrazol-1-yl)propan-1-one (**9**) was known to be the active isomer.

**Fluorescence Polarization (FP) Binding Assay**. A fluorescent polarization based binding assay was utilized using competition with a fluorescently labeled ATP competitive ligand (14-(2-([3-((2-([4-(cyanomethyl)phenyl]amino)-6-[(5-cyclopropyl-1H-pyrazol-3-yl)amino]-4-pyrimidinyl]amino)propyl]amino)-2-oxoethyl)-16,16,18,18-tetramethyl-6,7,7a,8a,9,10,16,18-octahydrobenzo[2'',3'']indolizino[8'',7'':5',6']pyrano[3',2':3,4]pyrido[1,2-*a*]indol-5-ium-2-

1  
2  
3 sulfonate. The assay was conducted as previously described and in the Supporting Information  
4  
5 with at least  $n = 2$  and the mean  $IC_{50}$  reported.<sup>15,16</sup>  
6

7  
8 **ADP-Glo Activity Assay.** The catalytic activity of RIP1 kinase was quantified utilizing the  
9  
10 Promega ADP-Glo kinase kit as previously described and in the Supporting Information using  
11  
12 either a four-parameter curve fit, or a tight binding curve fit for compounds whose potency was  
13  
14 less than the detection limit of the assay (~ half the enzyme concentration).<sup>15,16</sup> Data are presented  
15  
16 as the mean  $IC_{50}$  from at least  $n=2$  determinations.  
17  
18

19  
20 **U937 and L929 Cell Necroptosis Assay.** The efficacy of RIP1 kinase inhibitors were  
21  
22 determined in vitro using human monocytic leukemia U937 cells or mouse L-cells NCTC 929  
23  
24 (L929) cells in a necroptosis assay as previously described.<sup>15,16</sup>  
25

26  
27 **Biological in Vitro Whole Blood Assay.** Compound **77** was evaluated in a human whole blood  
28  
29 assay as previously described.<sup>16</sup> For the assay, 3 stock solutions each of 200 ng/mL TNF (Cell  
30  
31 Sciences), 400  $\mu$ M QVD-OPh or zVAD.fmk (R&D Systems) and 20  $\mu$ M 2',2''-(2,4-hexadiyne-  
32  
33 1,6-diyl)bis[1-[[[(2S)-1-(N-methyl-L-alanyl-L-threonyl)-2-pyrrolidinyl]methyl]-5-(phenylthio)-  
34  
35 1H-tetrazole (RMT 526529) were prepared in phenol red free RPMI 1640 medium supplemented  
36  
37 with 1% fetal bovine serum, 100 units/mL penicillin and 100  $\mu$ g/mL streptomycin. In addition, 5-  
38  
39 fold dilution series of compound **77** were prepared in the same medium supplemented with 1%  
40  
41 DMSO, with top concentrations of 1  $\mu$ M and 5  $\mu$ M for human and monkey assays, respectively.  
42  
43 A 5  $\mu$ L solution of compound **77** at each dilution was transferred to a 96 well tissue culture treated  
44  
45 assay plate and 5  $\mu$ L of each of the 3 stock solutions was added. Whole blood was collected by  
46  
47 venous puncture in heparin tubes (Griener Bio-One). Whole blood (80  $\mu$ L) was added to each well  
48  
49 of the assay plate, mixed briefly and incubated for 6 h at 37 °C, 5%  $CO_2$ . Following incubation,  
50  
51 PBS (200  $\mu$ L) was added to each well and the assay plate was centrifuged at 1700 rpm for 5 min.  
52  
53  
54  
55  
56  
57  
58  
59  
60

Supernatants were frozen at -70 °C. Concentrations of MIP-1 $\alpha$  (human) were determined by sandwich ELISA (Meso Scale Discovery) following the manufacturer's instructions.

**Biological in Vivo Assay.** The efficacy of RIP1 kinase inhibitors can be tested in mice in vivo using a TNF-driven systemic inflammatory response syndrome model, where injection of TNF combined with the caspase inhibitor zVAD-fmk leads to onset of a systemic inflammatory response in about 3 hours. A total of 7 mice per dose group were orally pre-dosed with vehicle (5% DMSO, 6% Cavitron in water) or compound **54** at doses of 1.4, 14 and 140 mg/kg 15 min before iv administration of zVAD-fmk (16.67 mg/kg) or mouse TNF $\alpha$ /zVAD-fmk at 1.25 mg/kg /16.67 mg/kg. Temperature loss in the mice was measured by rectal probe. The study was terminated after 3 hours when the control group lost 7 °C. All data are shown as means  $\pm$  standard error of the mean.

**Experimental Autoimmune Encephalomyelitis Mouse Model.** C57BL/6 mice were inoculated by using commercially available ready to use inoculum (EK-0115, Hooke Laboratories, USA) containing 100  $\mu$ g of MOG35-55, 200  $\mu$ g heat inactivated of Mycobacterium tuberculosis in mineral oil in 100  $\mu$ l of inoculum. Inoculation was done by giving each mouse 2 x 100  $\mu$ l injections subcutaneously to lower and higher aspect of the back. Intraperitoneal injections of pertussis toxin (4  $\mu$ g/ml) 100  $\mu$ l each were given at 2 hours and 24 hours after inoculation. Clinical signs were scored as follows: 0, no clinical signs; 0.5, partial tail weakness; 1, complete tail paralysis; 1.5, flaccid tail and abnormal gait; 2, flaccid tail and clear weakness of hind legs; 2.5, partial paralysis in one hind limb; 3, complete paralysis in both hindlimbs; 4, complete paralysis in hindlimbs and partial weakness in forelimbs; and 5, complete paralysis in both forelimbs and hindlimbs, moribund. Clinical scoring was performed by blinded observers. Mice were put on control and compound-treated diet one day prior to EAE induction.

**Rd10 Mouse Model of Human Retinitis Pigmentosa.** Rd10/rd10 pregnant dams were housed in darkness upon observation of a mucus plug. Newborn pups were housed with mothers in complete darkness from postnatal day 1 through postnatal day 30 (P1-P30). Mice were put on control and compound-treated diet on P29. On P31, animals were transitioned to maintenance under normal cyclical light conditions consisting of 12 hours of light (< 500 lux) followed by 12 hours of darkness. Electroretinography (ERG) measurements were performed on days P39 and P46. After a minimum of 12 hr dark adaptation, animals were anesthetized by intraperitoneal injection of 85 mg/kg ketamine and 14 mg/kg xylazine. Animal preparation was performed under a dim red light (< 50 lux). ERG analyses was performed using an Espion system from Diagnosys. For the assessment of scotopic response, a stimulus intensity of 40 (S) cd.s/m<sup>2</sup> was presented to the dark-adapted dilated eyes. To evaluate photopic response, animals were light adapted for 10 minutes, then presented a strobe flash to the dilated eyes with an intensity of 10 (S) cd.s/m<sup>2</sup>. A total of 25 repeated flashes and measurements were averaged to produce the final waveform.

**Metabolite identification.** Carried out for DHP **9** (20  $\mu$ M) in rat, dog, monkey, human liver microsomes (final protein concentration 1 mg/mL) fortified with cytosol (final protein concentration 2 mg/mL). Reactions were initiated with cofactors NADPH and UDPGA, and were incubated at 37 °C for 60 min. The reactions were stopped by addition of 3 volumes of MeCN and protein was precipitated by centrifugation. The supernatant was collected, dried under nitrogen and reconstituted with 30% MeCN before analyzing by LC/UV/MS.

**CHI (chromatographic hydrophobicity index) logD** Log D was calculated at pH 7.4 from the retention time (tR) observed in a fast gradient reverse-phase HPLC.<sup>24</sup>

All studies involving the use of animals were conducted after review by the GlaxoSmithKline (GSK) Institutional Animal Care and Use Committee and in accordance with the GSK Policy on the Care, Welfare and Treatment of Laboratory Animals.

## ASSOCIATED CONTENT

### Supporting Information

Preparation of DHPs **14-52**, **55-75**, enzyme preparations, RIP1 kinase co-crystallization of **11** and **77**, quantification of retinal thickness assessment for Rd10 in vivo model, kinase selectivity profile of DHP **9**, method and results of homology model of mouse RIP1 kinase with DHP **76** bound.

### Accession Codes

Coordinates and structure factors for the cocrystal structure of RIP1 kinase (1–294, C34A, C127A, C233A, C240A) and pyrrolidine **11** and dihydropyrazole **77** have been deposited in the Protein Data Bank with the accession numbers 6OCQ and 6R5F, respectively.

## AUTHOR INFORMATION

\*Corresponding Author e-mail: phaharris100@gmail.com

ORCID Philip A. Harris: 0000-0002-5189-3326

<sup>o</sup>Present Address for:

N.F. Institut de Recherches Servier, 11, Rue des Moulineaux, 92150 Suresnes, France.



N.G., V.B., A.D., F.D., M-H.F., P.Gr., E.J., P.L., F.P., S.S. Oncodesign, 25-27 avenue du Québec, 91951, Les Ulis cedex, France.

D.Y. Janssen Pharmaceutical Companies of Johnson & Johnson, 1400 McKean Rd, Spring House, PA 19477, USA.

S.C. Pharmaron, Drug Discovery Services Europe, Hertford Road, Hoddesdon, Hertfordshire, EN11 9BU, UK.

The authors declare the following competing financial interests: All authors, with the exception of Veronique Beneton, Deepak Bandyopadhyay, Sebastien Campos, Alain Daugan, Frederic Donche, Nicolas Faucher, Marie-Hélène Fouchet Nicolas George, Pascal Grondin. Emilie Jigorel, Pauline Lamoureux, Julie E Mosley, Pam M Nassau, Florent Potvain and Stephane Sautet, are current employees and stockholders of GlaxoSmithKline.

## ACKNOWLEDGMENTS

The authors would like to thank Alexis Denis, Tony Cooper and Vipul Patel for their help and discussions during the course of this work, and Mui Cheung for reviewing the manuscript.

## ABBREVIATIONS USED

ANOVA, analysis of variance; BOC, *tert*-butoxycarbonyl; DFG, Asp-Phe-Gly; DLG, Asp-Leu-Gly; DCM, dichloromethane; DHP, dihydropyrazole; DIBAL-H, diisobutylaluminium hydride; DIPEA, diisopropylethylamine; EAE, experimental autoimmune encephalomyelitis, FasL, Fas ligand; FaSSIF, fasted state simulated intestinal fluid; FP, fluorescence polarization; HATU, 1-[bis(dimethylamino)methylene]-1H-1,2,3-triazolo[4,5-b]pyridinium 3-oxide

hexafluorophosphate; MIP, macrophage inflammatory protein; RIP1, receptor interacting protein 1; QVD-OPh, (3S)-5-(2,6-difluorophenoxy)-3-[[[(2S)-3-methyl-1-oxo-2-[(2-quinolinylcarbonyl)amino]butyl]amino]-4-oxopentanoic acid hydrate; SMAC, second mitochondrial-derived activator of caspases; T3P, 2,4,6-tripropyl-1,3,5,2,4,6-trioxatriphosphinane 2,4,6-trioxide; TEA, triethylamine; TNF, tumor necrosis factor; TNFR1, tumor necrosis factor receptor 1; TRAIL, TNF-related apoptosis-inducing ligand; zVAD.fmk, carbobenzoxy-valyl-alanyl-aspartyl-[O-methyl]- fluoromethylketone.

## REFERENCES

1. Berger, S. B.; Kasparcova, V.; Hoffman, S.; Swift, B.; Dare, L.; Schaeffer, M.; Capriotti, C.; Cookm M.; Finger, J.; Hughes-Earle, A.; Harris, P. A.; Kaiser, W. J.; Mocarski E. S.; Bertin, J.; Gough, P. J. Cutting Edge: RIP1 Kinase Activity is Dispensable for Normal Development but is a Key Regulator of Inflammation in SHARPIN-Deficient Mice. *J. Immunol.* 2014, 192, 5476-5480.
2. Takahashi, N.; Vereecke, L.; Bertrand, M. J. M.; Duprez, L.; Berger, S. B.; Divert, T.; Goncalves, A.; Sze, M.; Gilbert, B.; Kourula, S.; Goossens, V.; Lefebvre, S.; Gunther, C.; Becker, C.; Bertin, J.; Gough, P. J.; Declercq, W.; van Loo, G.; Vandenabeele, P. RIPK1 Ensures Intestinal Homeostasis by Protecting the Epithelium Against Apoptosis. *Nature* 2014 513, 95-99.
3. Dannappel, M.; Vlantis, K.; Kumari, S.; Polykratis, A.; Kim, C.; Wachsmuth, L.; Eftychi, C.; Lin, J.; Corona, T.; Hermance, N.; Zelic, M.; Kirsch, P.; Basic, M.; Bleich, A.; Kelliher, M.; Pasparakis M. RIPK1 Maintains Epithelial Homeostasis by Inhibiting Apoptosis and Necroptosis. *Nature* 2014 513, 90-94.

4. Pasparakis, M.; Vandenabeele, P. Necroptosis and its Role in inflammation. *Nature* 2015, 517, 311-320.
5. Jouan-Lanhouet, S.; Arshad, M. I.; Piquet-Pellorce, C.; Martin-Chouly, C.; Le Moigne-Muller, G.; Van Herreweghe, F.; Takahashi, N.; Sergent, O.; Lagadic-Gossmann, D.; Vandenabeele, P.; Samson, M.; Dimanche-Boitrel, M. T. TRAIL Induces Necroptosis Involving RIPK1/RIPK3-Dependent PARP-1 Activation. *Cell Death Differ.* 2012, 19, 2003-2014.
6. Najjar, M.; Saleh, D.; Zelic, M.; Nogusa, S.; Shah, S.; Tai, A.; Finger, J. N.; Polykratis, A.; Gough, P. J.; Bertin, J.; Whalen, M. J.; Pasparakis, M.; Balachandran, S.; Kelliher, M.; Poltorak, A.; Degterev, A. RIPK1 and RIPK3 Kinases Promote Cell-Death Independent Inflammation by Toll-Like Receptor 4. *Immunity* 2016, 45, 46-59.
7. McNeal, S. I.; LeGolván, M. P.; Chung, C. S.; Ayala, A. The Dual Functions of RIP1 in FAS-induced Hepatocyte Death During Sepsis. *Shock* 2011, 35, 499-505.
8. Berger, S. B.; Gough, P. J.; Bertin, J. Life After Death: RIP1 and RIP3 Move Beyond Necroptosis. *Cell Death Dis.* 2016, 2, 16056.
9. Newton, K.; Dugger, D. L.; Maltzman, A.; Greve, J. M.; Hedehus, M.; Martin-McNulty, B.; Carano, R. A. D.; Cao, T. C.; van Bruggen, N.; Bernstein, L.; Lee, W. P.; Wu, X.; DeVoss, J.; Zhang, J.; Jeet, S.; Peng, I.; McKenzie, B. S.; Roose-Girma, M.; Caplazi, P.; Diehl, L.; Webster, J. D.; Vucic, D. RIPK3 Deficiency or Catalytically Inactive RIPK1 Provides Greater Benefit Than MLKL Deficiency in Mouse Models of Inflammation and Tissue Injury. *Cell Death Differ.* 2016, 23, 1565-1576.

10. Degterev, A.; Hitomi, J.; Gemscheid, M.; Ch'en, I. L.; Korkina, O.; Teng, X.; Abbott, D.; Cuny, G. D.; Yuan, C.; Wagner, G.; Hedrick, S. M.; Gerber, S. A.; Lugovskoy, A.; Yuan, J. Identification of RIP1 Kinase as a Specific Cellular Target of Necrostatins. *Nat. Chem. Biol.* 2008, 4, 313-321.
11. Degterev, A.; Huang, Z.; Boyce, M.; Li, Y.; Jagtap, P.; Mizushima, N.; Cuny, G. D.; Mitchison, T. J.; Moskowitz M. A.; Yuan J. Chemical Inhibitor of Nonapoptotic Cell Death With Therapeutic Potential for Ischemic Brain Injury. *Nat. Chem. Biol.* 2005, 1, 112-119.
12. Xie, T.; Peng, W.; Liu, Y.; Yan, C.; Maki, J.; Degterev, A.; Yuan, J.; Shi Y. Structural Basis of RIP1 Inhibition by Necrostatins. *Structure* 2013, 21, 493-499.
13. Christofferson, D. E.; Li, Y.; Hitomi, J.; Zhou, W.; Upperman, C.; Zhu, H.; Gerber, S. A.; Gygi, S.; Yuan J. A Novel Role for RIP1 Kinase in Mediating TNF $\alpha$  Production. *Cell Death Dis.* 2012, 3,e320.
14. Harris, P. A.; Bandyopadhyay, D.; Berger, S. B.; Campobasso, N.; Capriotti, C. A.; Cox, J. A.; Dare, L.; Finger, J. N.; Hoffman, S. J.; Kahler, K. M.; Lehr, R.; Lich, J. D.; Nagilla, R.; Nolte, R. T.; Ouellette, M. T.; Pao, C. S.; Schaeffer, M. C.; Smallwood, A.; Sun, H. H.; Swift, B. A.; Totoritis, R. D.; Ward, P.; Marquis, R. W.; Bertin, J.; Gough, P. J. Discovery of Small Molecule RIP1 Kinase Inhibitors for the Treatment of Pathologies Associated With Necroptosis. *ACS Med. Chem. Lett.* 2013, 4, 1238-1243.
15. Harris, P. A.; King, B. W.; Bandyopadhyay, D.; Berger, S. B.; Campobasso, N.; Capriotti, C. A.; Cox, J. A.; Dare, L.; Dong, X.; Finger, J. N.; Grady, L. C.; Hoffman, S. J.; Jeong, J. U.; Kang, J.; Kasparcova, V.; Lakdawala, A. S.; Lehr, R.; McNulty, D.E.; Nagilla, R.; Ouellette, M. T.; Pao, C. S.; Rendina, A. R.; Schaeffer, M. C.; Summerfield, J. D.; Swift, B.A.; Totoritis,

- R.D.; Ward, P.; Zhang, A.; Zhang, D.; Marquis, R. W.; Bertin, J.; Gough, P. J. DNA-Encoded Library Screening Identifies Benzo[1,4]Oxazepin-4-Ones as Highly Potent and Monoselective Receptor Interacting Protein 1 Kinase Inhibitors. *J. Med. Chem.* 2016, 59, 2163-2178.
16. Harris, P. A.; Berger, S. B.; Jeong, J. U.; Nagilla, R.; Bandyopadhyay, D.; Campobasso, N.; Capriotti, C. A.; Cox, J. A.; Dare, L.; Dong, X.; Eidam, P. M.; Finger, J. N.; Hoffman, S. J.; Kang, J.; Kasparcova, V.; King, B. W.; Lehr, R.; Lan, Y.; Leister, L. K.; Lich, J. D.; MacDonald, T. T.; Miller, N. A.; Ouellette, M. T.; Pao, C. S.; Rahman, A.; Reilly, M. A.; Rendina, A. R.; Rivera, E. J.; Schaeffer, M. C.; Sehon, C. A.; Singhaus, R. R.; Sun, H. H.; Swift, B. A.; Totoritis, R. D.; Vossenkämper, A.; Ward, P.; Wisnoski, D. D.; Zhang, D.; Marquis, R. W.; Gough P. J.; Bertin, J. Discovery of a First-in-Class Receptor Interacting Protein 1 (RIP1) Kinase Specific Clinical Candidate (GSK2982772) for the Treatment of Inflammatory Diseases. *J. Med. Chem.* 2017, 60, 1247–1261.
17. Yoshikawa, M.; Saitoh, M.; Katoh, T.; Seki, T.; Bigi, S. V.; Shimizu, Y.; Ishii, T.; Okai, T.; Kuno, M.; Hattori, H.; Watanabe, E.; Saikatendu, K. S.; Zou, H.; Nakakariya, M.; Tatamiya, T.; Nakada, Y.; Yogo, T. Discovery of 7-Oxo-2,4,5,7-tetrahydro-6 H-pyrazolo[3,4- c]pyridine Derivatives as Potent, Orally Available, and Brain-Penetrating Receptor Interacting Protein 1 (RIP1) Kinase Inhibitors: Analysis of Structure-Kinetic Relationships. *J. Med. Chem.* 2018, 61, 2384-2409.
18. Berger, S. B.; Harris, P.; Kasparcova, K.; Hoffman, S.; Swift, B.; Dare, L.; Schaeffer, M.; Capriotti, C.; Ouellette, M.; King, B. W.; Wisnoski, D.; Cox, J.; Relly, M.; Marquis, R. W.; Bertin, J.; Gough, P. J. Characterization of GSK'963: a Structurally Distinct, Potent and Selective Inhibitor of RIP1 Kinase. *Cell Death Disc.* 2015, 1, 15009.

19. Zhang, Z.; Wang, X.; Su, Y.; Ruan, H.; Ren, Y. Necrosis Inhibitors. *PCT Int. Appl.* WO2016101887, June 30, 2016.
20. Duprez, L.; Takahashi, N.; Van Hauwermeiren, F.; Vandendriessche, B.; Goossens, V.; Vanden Berghe, T.; Declercq, W.; Libert, C.; Cauwels, A.; Vandenabeele, P. RIP Kinase-Dependent Necrosis Drives Lethal Systemic Inflammatory Response Syndrome. *Immunity* 2011, 35, 908–918.
21. Li, L.; Thomas, R. M.; Suzuki, H.; De Brabander, J. K.; Wang, X.; Harran, P. G. A Small Molecule Smac Mimic Potentiates TRAIL- and TNF $\alpha$ -mediated Cell Death. *Science* 2004, 305, 1471-1474.
22. Ofengeim, D.; Ito, Y.; Najafov, A.; Zhang, Y.; Shan, B.; DeWitt, J. P.; Ye, J.; Zhang, X.; Chang, A.; Vakifahmetoglu-Norberg, H.; Geng, J.; Py, B.; Zhou, W.; Amin, P.; Berlink Lima, J.; Qi, C.; Yu, Q.; Trapp, B.; Yuan, J. Activation of Necroptosis in Multiple Sclerosis. *Cell Rep.* 2015, 10, 1836–1849.
23. Chang, B.; Hawes, N. L.; Pardue, M. T.; German, A. M.; Hurd, R. E.; Davisson, M. T.; Nusinowitz, S.; Rengarajan, K.; Boyd, A. P.; Sidney, S. S.; Phillips, M. J.; Stewart, R. E.; Chaudhury, R.; Nickerson, J. M.; Heckenlively, J. R.; Boatright, J. H. Two Mouse Retinal Degenerations Caused by Missense Mutations in the Beta-Subunit of Rod Cgmp Phosphodiesterase Gene. *Vision Res.* 2007, 47, 624-33.
24. Valkó, K. Chromatographic Hydrophobicity Index by Fast-gradient RP-HPLC: a High-throughput Alternative to Log P/Log D. *Anal. Chem.* 1997, 69, 2022–2029.

## Table of Contents graphic

